Mon. Not. R. Astron. Soc. **000**, 1–15 (2015) Printed 27 August 2015 (MN LaTeX style file v2.2)

The OmegaWhite Survey for Short-Period Variable Stars I: Overview and First Results

S.A Macfarlane[1,2⋆], R. Toma[3], G. Ramsay[3], P.J Groot[1], P.A Woudt[2], J.E Drew[4], G. Barentsen[4], J. Eislöffel[5],

[1] *Department of Astrophysics/IMAPP, Radboud University, P.O. Box 9010, 6500 GL Nijmegen, The Netherlands*
[2] *Astrophysics,Cosmology and Gravity Centre, Department of Astronomy, University of Cape Town, Private Bag X3, Rondebosch 7701, South Africa*
[3] *Armagh Observatory, College Hill, Armagh, BT61 9DG, Northern Ireland*
[4] *School of Physics, Astronomy & Mathematics, University of Hertfordshire, College Lane, Hatfield, Hertfordshire, AL10 9AB, U.K.*
[5] *Thüringer Landessternwarte, Sternwarte 5, D-07778 Tautenburg, Germany*

27 August 2015

ABSTRACT

We present the goals, strategy and first results of the OmegaWhite survey: a wide-field high-cadence g-band synoptic survey which aims to unveil the Galactic population of short-period variable stars (with periods < 80 min), including ultracompact binary star systems and stellar pulsators. The ultimate goal of OmegaWhite is to cover 400 square degrees along the Galactic Plane reaching a depth of $g = 21.5$ mag (10σ), using OmegaCam on the VLT Survey Telescope (VST). The fields are selected to overlap with surveys such as the Galactic Bulge Survey (GBS) and the VST Photometric Hα Survey of the Southern Galactic Plane (VPHAS+) for multi-band colour information. Each field is observed using 38 exposures of 39 s each, with a median cadence of $\sim$2.7 min for a total duration of two hours. Within an initial 26 square degrees, we have extracted the light curves of 1.6 million stars, and have identified 613 variable candidates which satisfy our selection criteria. Furthermore, we present the light curves and statistical properties of 20 sources which have the highest-likelihood of being variable stars. One of these candidates exhibits the colours and light curve properties typically associated with ultracompact AM CVn binaries, although its spectrum exhibits weak Balmer absorption lines and is thus not likely to be such a binary system. We also present follow-up spectroscopy of five other variable candidates, which identifies them as likely low-amplitude δ Sct pulsating stars.

Key words: surveys – binaries: close – Galaxy:bulge – methods: observational – methods: data analysis – techniques: photometric.

1 INTRODUCTION

Time domain astrophysics has been transformed over the last decade. Whereas in the past, photometric data of individual objects were painstakingly obtained using high speed photometry or dedicated long term projects, now a whole series of synoptic projects have been developed to observe large areas of sky over short time-scales giving photometric data on thousands or millions of objects. The diversity of goals of these projects is considerable, ranging from detecting transiting exo-planets (e.g. the main aim of the 'SuperWASP' project, Pollacco et al. 2006) to discovering supernova outbursts (e.g. supernova discoveries in the Palomar Transient Factory (PTF), Law et al. 2009).

In the field of Galactic binary research, one key goal has been to discover individual systems with astrophysically interesting properties. Of particular interest are ultracompact binaries (UCBs) which have an orbital period (P_{orb}) of $\leqslant$ 70 min, implying that the secondary star cannot be a main-sequence star (Rappaport et al. 1982). Furthermore, these hydrogen-deficient objects are predicted to be the strongest known sources of gravitational wave radiation (GWR) in the passband of the satellite observatory *eLISA* (Amaro-Seoane et al. 2013; Roelofs et al. 2007), and as such are important calibrators that provide verification of the existence and detectability of GWR. Moreover, the evolution of these binary

⋆ Email: S.Macfarlane@astro.ru.nl

Table 1. Overview of recent high-cadence synoptic surveys

Survey	Field Location (deg)	Total Sky Coverage (deg^2)	Depth (V mag)	Variability sensitivity (min)
OmegaWhite[a]	$\|b\| \leqslant 10$	400	21.5	> 6
RATS[b]	$\|b\| \leqslant 30$	46	22.5	> 5
RATS-Kepler[c]	$6 \leqslant \|b\| \leqslant 21$	49	22.5	> 5
FSVS[d]	$\|b\| \geqslant 20$	23	24.0	> 24
DLS[e]	$\|b\| < 10$	21	25.5	> 15
Kepler[f]	$15 \leqslant \|b\| \leqslant 25$	116	20.0	> 1 or > 30
SuperWASP[g]	all sky	all sky	15.0	> 10

[a]This paper, [b]Rapid Temporal Survey (Ramsay & Hakala 2005), [c](Ramsay et al. 2014), [d]Faint Sky Variability Survey (Groot et al. 2003), Deep Lens Survey [e](Becker et al. 2004), [f] (Borucki et al. 2010), [g]Wide Angle Search for Planets (Pollacco et al. 2006)

systems is influenced by the emission of GWR in addition to the mass transfer phase. Therefore, the study of UCBs will also help to answer key questions of late-stage binary evolution. Earlier estimates of their intrinsic numbers suggested a relatively high foreground contribution from UCBs to the gravitational wave signal from merging supermassive black holes within the *eLISA* band. However, in a series of papers using SDSS and PTF data (Roelofs et al. 2009; Rau et al. 2010; Carter et al. 2013; Levitan et al. 2015), it is now clear that the predicted number density of AM CVn binaries (semi-detached and mass transferring UCBs) in the Solar neighbourhood is $5 \pm 3 \times 10^{-7} \mathrm{pc}^{-3}$, a factor 50 lower than previous estimates by Nelemans et al. (2001). Other surveys which have recently had success in discovering new AM CVn systems include the Catalina Real-Time Transient Survey (CRTS Drake et al. 2009), and the All Sky Automated Survey for Supernovae (ASAS-SN, e.g. Wagner et al. 2014).

The emission line method for finding AM CVn systems, on which the SDSS work is based, is most sensitive to systems with $P_{orb} \geqslant 30$ min. More recently, the PTF survey has been identifying outbursting AM CVns which have orbital periods shorter than this, but still greater than 22 min (Levitan et al. 2015). From the total number of 43 known AM CVns, only 6 have periods shorter than 20 minutes. It is those systems with the shortest orbital period (5 min $< P_{orb} <$ 20 min) which are predicted to be the strongest emitters of gravitational waves. Determining their population size is important for both the development of *eLISA* and for deducing the relative importance of the three postulated formation channels of these binaries (for a detailed review, see Solheim 2010). A way to identify those AM CVn stars with the shortest orbital periods is through their photometric behaviour as they show a periodic modulation on, or close to, the orbital period (e.g. the first PTF AM CVn discovered, Levitan et al. 2011). Variations are expected due to eclipses, ellipsoidal variations, irradiation, superhumps, or anisotropic disc hotspot emission in the system. The detection of these especially short-period systems is the main motivation behind the OmegaWhite survey.

However, short time-scale photometric variations can also originate from physical changes within the internal structure or atmosphere of the source. Examples of such sources include flare stars or fast pulsating stars such as δ Scuti stars (δ Sct, Breger 2000) or SX Phoenicis variables (e.g. Rodríguez & López-González 2000). At even shorter periods, rapidly oscillating Ap or Am star systems (roAp, roAm), and pulsating white dwarfs (ZZ Ceti variables) exhibit periodic variations on amplitudes ranging from a percent or less up to several tens of percent on timescales of a few to tens of minutes.

δ Sct stars have A–F spectral types and are known to have short pulsation periods (typically 0.02 - 0.25 days, Chang et al. 2013), with absolute magnitudes 3 - 5 mag fainter than Cepheids. However, they are believed to be the second most common variable stars in the Galaxy (Breger 1979), and their short period makes them relatively easy to detect in high-cadence surveys (e.g. Ramsay & Hakala 2005). δ Sct stars can be used as precise distance tracers if the fundamental radial pulsation mode can be identified (e.g. Petersen & Christensen-Dalsgaard 1999; McNamara et al. 2007). For high-amplitude δ Sct stars (HADS), where the pulsation amplitude is greater than 0.3 mag, it is expected that the dominant period will be due to the fundamental or first-overtone radial mode. The shortest period δ Sct stars in the Galactic field have a dominant pulsation period of $\sim$26 min (Kim et al. 2010).

One survey that set out to discover short-period systems was the Rapid Temporal Survey (RATS, Ramsay & Hakala 2005; Barclay et al. 2011). RATS was carried out using the 2.5-m Isaac Newton Telescope (INT) on La Palma and the 2.2-m Max Planck Gesellschaft telescope (MPG/ESO) between 2003–2010, and covered a total of 46 square degrees favouring fields near the Galactic plane. The fact that no AM CVn was discovered was (in retrospect) not a surprise since the latest space densities imply that only a few systems (at best) are expected in a survey covering this area. However, the survey did discover many new and interesting short-period variables, including a possible hybrid sdBV pulsator exhibiting long-period g-modes (Ramsay et al. 2006) and a dwarf nova discovered through its high-amplitude quasi-periodic oscillations (QPOs) in quiescence (Ramsay et al. 2009).

The OmegaWhite Survey, which is now being conducted using OmegaCam on the VST, has a similar observing strategy to RATS (See Table 1 for a comparison of similar stellar wide-field surveys). However, OmegaWhite aims to cover a much wider area (400 square degrees) at lower average Galactic latitudes ($|b| < 5$ degrees). In this paper we present: the OmegaWhite observing strategy, the reduction pipeline, our method for identifying objects of interest, an outline of those variables identified in ESO semester 88 (Dec. 2011 –

Table 2. OmegaWhite observation log for observations made between December 2011 and April 2015

ESO Period	Observation Dates	Allocated Time (hrs)	Observed Fields (hrs)	RA (J2000) (hh:mm)	DEC (J2000) (°:′)
88	Dec. 2011 to Apr. 2012	32	28	07:35 – 08:25	–30:00 – –26:00
90	Nov. 2012 to Mar. 2013	64	8	07:05 – 08:25	–30:00 – –25:00
91	Apr. 2013 to Sep. 2013	64	36	17:00 – 18:25	–29:30 – –23:30
92	Dec. 2013 to Apr. 2014	48	6	07:05 – 08:40	–31:00 – –26:00
93	Apr. 2014 to Sep. 2014	80	36	17:05 – 18:30	–32:30 – –21:30
94	Dec. 2015 to Apr. 2015	64	34	07:15 – 08:30	–33:00 – –22:00

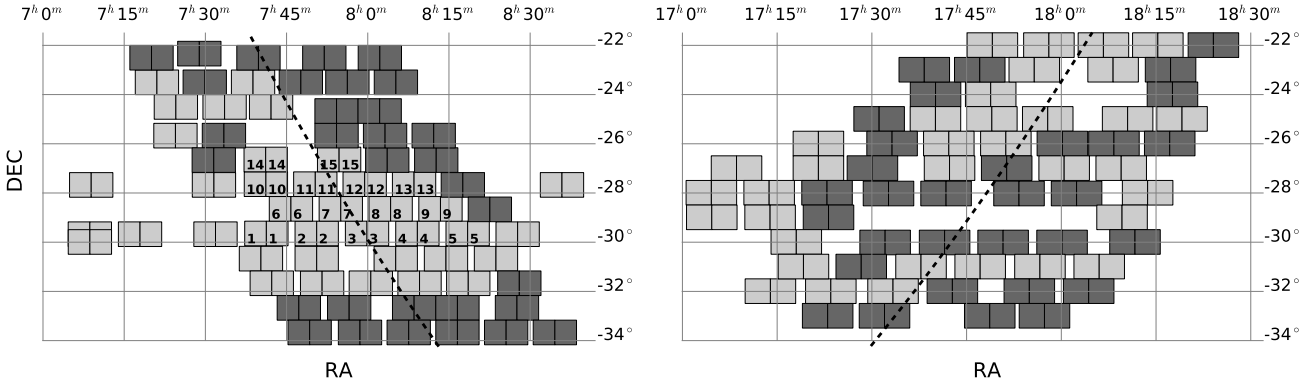

Figure 1. The two regions of OmegaWhite field pointings along the Galactic plane (dashed line), including the Galactic Bulge region (right panel). Fields are either observed (light grey, both panels), scheduled for semester 95 (dark grey, right panel), or scheduled for semester 96 (dark grey, left panel). Semester 88 field pairs are indicated by their identification number, and their respective co-ordinates are listed in Table A1.

Apr. 2012), and a discussion of the science goals which can be investigated using these data.

2 OBSERVATIONS

OmegaWhite observations are taken in g-band using the wide-field instrument OmegaCAM (Kuijken 2011) on the VLT Survey Telescope (VST, Capaccioli & Schipani 2011). The VST is a 2.65-m wide-field survey telescope situated at the ESO Paranal Observatory in Northern Chile. The sole instrument on the telescope, OmegaCAM is a 16k × 16k imaging camera, covering one square degree with 32 CCDs (each 2k × 4k) at a plate scale of 0.216 arcsec/pixel.

The OmegaWhite survey targets 400 square degrees along the Galactic plane ($|b| < 5$ degrees) and Galactic bulge ($|l|$,$|b| < 10$ degrees), of which 148 fields (equivalent to 148 square degrees) have been observed during ESO semesters 88 to 94 (see Table 2 for semester details, and Figure 1 for pointing locations). OmegaWhite fields were chosen to overlap with the VST Photometric Hα Survey of the Southern Galactic Plane (VPHAS+, Drew et al. 2014) and the Galactic Bulge Survey (GBS, Jonker et al. 2011) pointings in order to obtain broad-band colours and photometric zeropoints, whilst avoiding bright stars ($V < 5$ mag).

2.1 Observing Strategy

The OmegaWhite observing strategy has been primarily designed to detect binary stars with orbital periods in the 5 to 60 minute range, whilst optimising the compromise between sky coverage and cadence. Two neighbouring one square degree fields are alternatingly observed in 39 second exposures over an observing duration of 2 hours, with an observational median cadence of ∼2.7 minutes per field. Thus 38 exposures per field are obtained. From the Faint Sky Variability Survey (FSVS Groot et al. 2003), it was determined that ∼25 observations are necessary in order to reliably identify and accurately determine the period of short-period variables (Morales-Rueda et al. 2006). Furthermore, this exposure time allows for observations to reach magnitude limits of $g \approx 21.5$ (10σ) per exposure. Much deeper than this is, at times, not useful in the Galactic Plane with seeing-limited ground-based observations due to stellar crowding. Also, it is unlikely that we will get astrophysically useful identification/follow-up spectra for sources fainter than $g \approx$ 21 mag.

Every two hour observation consists of five observing blocks, each having a respective duration of 21 min, 29 min, 20 min, 21 min, and 29 min (in sequential order). The irregular durations help break any aliasing that may arise from regular scheduling. At the start of every observing block, the field is reacquired for refocusing and image analysis purposes. For our observations, the seeing is $\leqslant 1''$ with clear to thin cloud conditions at the start. However, we are required to relax these constraints for the two observing blocks starting after one hour. Specifically, the seeing is allowed to increase to $2''$ and thick cloud cover is accepted.

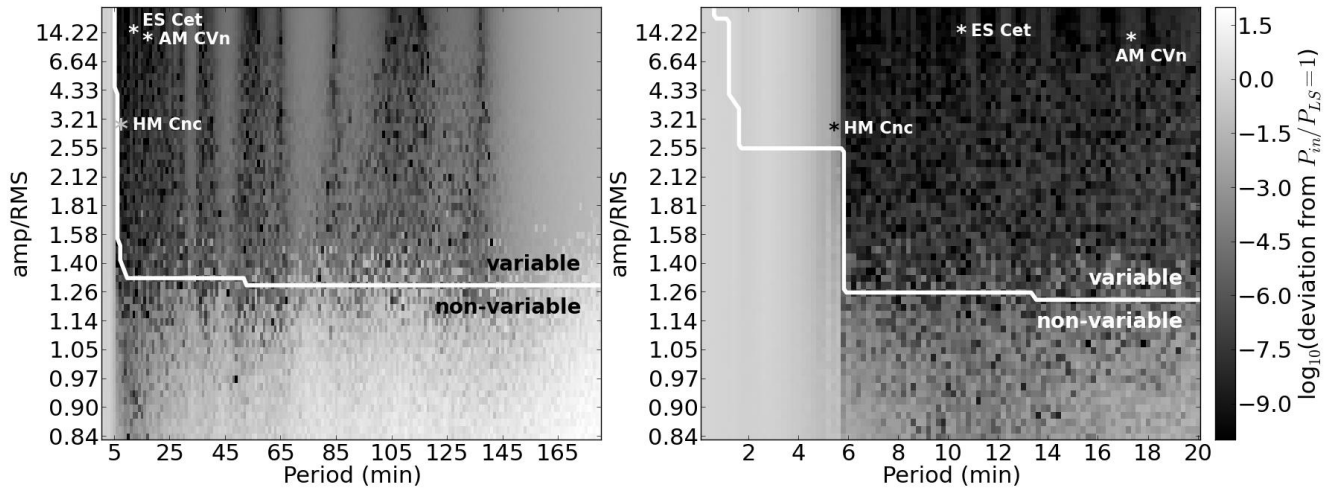

Figure 2. The logarithmic absolute deviation from $P_{in}/P_{LS} = 1$, in period (P_{in}) and amp/RMS space, sampled in one minute period bins (left panel), and in 0.2 minute period bins (right panel). The region above and to the right of the white solid line indicates where sources have $\log_{10}(\mathrm{FAP}) < -2.5$, and are therefore considered variable at the 3σ level. The location of three short period (HM Cnc, ES Cet, and AM CVn) are each indicated by a star in both panels.

2.2 Simulations

A key question is whether we can detect the variability of short-period systems (such as AM CVn binaries) using our current observing strategy and statistical analysis tools. We applied the VARTOOLS suite of software (Hartman et al. 2008, used for variability statistics, see Section 3.4) to the light curves of our OmegaWhite sources, allowing us to determine their respective output Lomb Scargle Period (P_{LS}), as well as their false alarm probability (FAP). A light curve with $\log_{10}(\mathrm{FAP}) = -2.5$ is likely to be variable at the 3σ confidence level, and the more negative $\log_{10}(\mathrm{FAP})$ is, the more likely it is that the source is variable (see Section 3.4 for more details).

We simulated variable OmegaWhite light curves by applying the actual observing sequence (as outlined in Section 2.1) to basic sinusoidal waveforms with increasing input periods (P_{in}) in the range 1 min $\leqslant P_{in} \leqslant$ 180 min. To model the intensity of each exposure, we integrated the sine wave over the corresponding exposure time interval, to which we then added random Gaussian noise. For the Gaussian sigma level, we used the root mean square (RMS) of the magnitude of a sample of observed light curves, calculating how the standard deviation of the mean for each non-variable light curve in the example field 'OW_88D_1a' varies as a function of the source's magnitude. We then applied VARTOOLS to the light curves, allowing us to determine P_{LS} and the FAP value for each P_{in}. Since the probability of finding our target systems depends on both the variability amplitude of the light curve (amp) and the RMS (which determines the noise level), we ran our simulations for a range of RMS to amp ratios (amp/RMS, where $0.01 <$ amp/RMS < 20.00).

In Figure 2, we show the logarithmic absolute deviation from $P_{in}/P_{LS} = 1$ for each simulated light curve in amp/RMS and $\log_{10}(\mathrm{FAP})$ space. The right panel focuses on the initial 20 minutes of the period range shown in the left panel, and is sampled at a higher rate (in 0.2 minute intervals, as opposed to the 1 minute intervals in the left panel). In both panels, we overlay a cutoff line to indicate the regions where OmegaWhite sources are variable at the 3σ level, with $\log_{10}(\mathrm{FAP}) < -2.5$ (upper right region).

Table 3. Properties of three short-period AM CVn systems

AM CVn	P_{orb} (min)	V (mag)	amp (mag)	amp/RMS	Ref.
HM Cnc	5.36	21.1	0.150	3	1,2
ES Cet	10.3	17.1	0.075	15	3
AM CVn	17.1	14.0	0.016	13	4,5,6

References: (1) Israel et al. (1999); (2) Ramsay et al. (2002); (3) Warner & Woudt (2002); (4) Smak (1967); (5) Warner & Robinson (1972); (6) Roelofs et al. (2006)

Therefore, using our observing strategy, we can expect to detect variable sources if they have properties which have amp/RMS $\geqslant 1.3$ and $P_{in} \geqslant 5.8$ min. Variable sources with $P_{in} \geqslant 1.6$ min should be detected provided they have amp/RMS $\geqslant 2.5$. Additionally, we found that the absolute deviation from $P_{in}/P_{LS} = 1$ increases for $P_{in} \leqslant 5.8$ min and for $P_{in} \geqslant 140$ min. Thus P_{LS} will overestimate P_{in} for sources with $P_{in} \leqslant 5.8$ min, and P_{LS} will overestimate P_{in} for sources with $P_{in} \geqslant 140$ min.

We applied our observing strategy and VARTOOLS to simulated light curves of three known short-period AM CVn systems (HM Cnc, ES Cet and, AM CVn, see Table 3 for system properties). As shown in Figure 2, the resultant P_{LS} and $\log_{10}(\mathrm{FAP})$ imply that we should be able to detect all three AM CVn systems as significantly variable with $\log_{10}(\mathrm{FAP}) < -2.5$ (although we will likely overestimate the P_{orb} of HM Cnc).

3 DATA ANALYSIS

Our pipeline for cleaning the raw data from instrumental effects, extracting the light curves and identifying variable

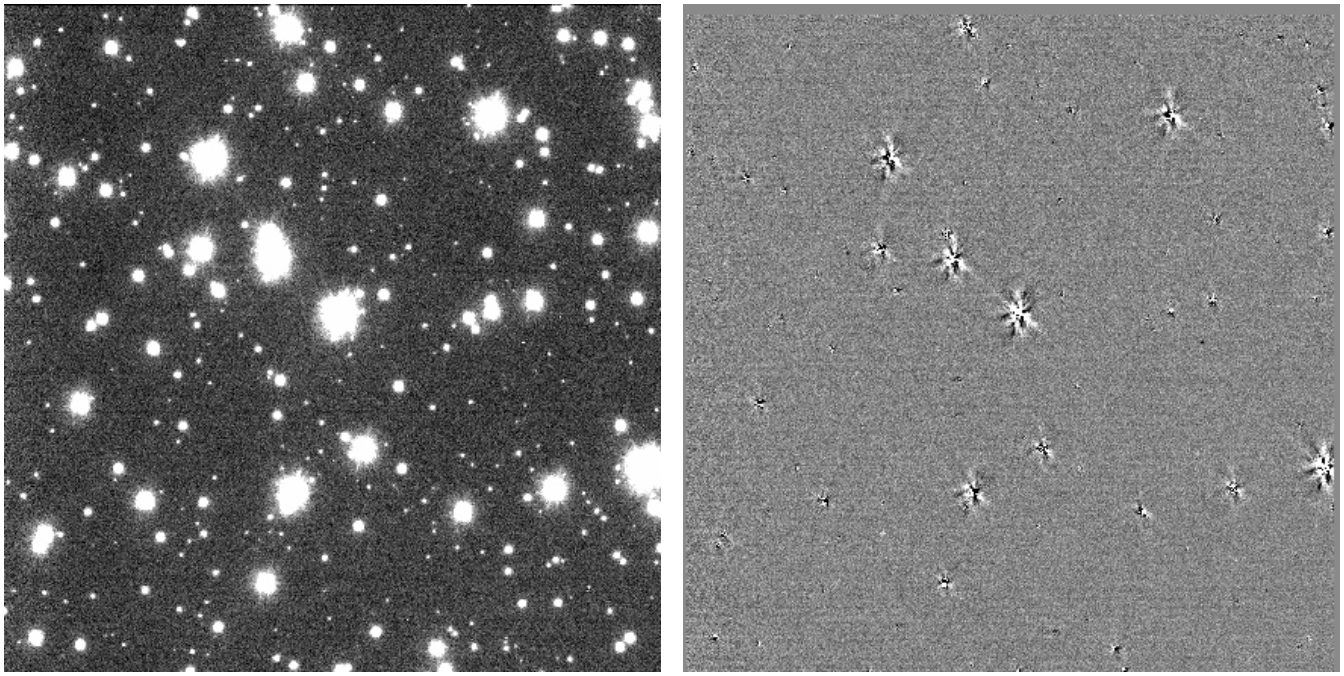

(a) Reference subframe (b) Difference subframe

Figure 3. Difference subframe (right panel) obtained after the reference subframe (left panel) is convolved and then subtracted from an individual science subframe. Each subframe is $3.75' \times 3.75'$. The residuals visible on the difference frame were caused by saturated stars.

stars is a modified version of that used by the RATS (Barclay et al. 2011) and RATS-Kepler (Ramsay et al. 2014) surveys. Here we give an overview of our procedure.

3.1 Image reduction and astrometric calibration

Median bias frames were created for each night, and a median g-band flat field, made using twilight fields, was created for every month for which science images were available (because flat field data were not acquired for every night). The raw science images were then cleaned using standard procedures through bias subtraction and flat field division. We notice the 'negative cross-talk' effect on frames from some chips - mostly on Chip #96 (Kuijken 2011; Drew et al. 2014).

Until early 2014, the VST has suffered various technical problems which caused the appearance of scattered light on many images. These issues were only resolved once baffles had been fit to the telescope (see Drew et al. 2014 for more details). On semester 88 data, we also found that the autoguiding did not achieve sufficient precision to ensure that stars were kept fixed on the same set of pixels over the course of observations. This problem, combined with the potentially variable sky background, would degrade the resulting photometry. Therefore, we expect that the photometry derived from semester 94 and onwards (see Table 2) would be significantly improved compared to the results from earlier semesters.

World coordinates were embedded using `Astrometry.net` software (Lang et al. 2010). This approach matches the sky position of stars in an image with a set of reference 'index' files created using data from the Two Micron All Sky Survey (2MASS, Jarrett et al. 2000), which are split according to the field's position in the sky and the known angular scale of the image. Initially, we used the software default index files. However, in crowded stellar fields (as we can find in our data), the astrometric solution led to discrepancies of several arcseconds between the fitted and known positions of 2MASS, or the software failed to find a solution for images of some chips. We sought to solve this problem by setting a brighter magnitude limit on the 2MASS reference stars, as brighter objects are less affected by crowding with faint sources. To implement this solution, we created our customised index files using stars within the field of OmegaCam, as well as 2MASS data (the default angular extent of the 2MASS index files is much greater than the field of view of OmegaWhite). Additionally, we filtered the 2MASS data to include only stars whose J-mag photometry has a signal-to-noise ratio greater than five, giving a limit of $J \sim 16.5$ mag (whereas the default files tend to go deeper). Our approach led to improved astrometric solutions for all chips with a typical residual of $\sigma \sim 0.1''$ in right ascension (RA) and declination (DEC) when compared to the 2MASS positions. Nevertheless, for a small number of fields which are particularly crowded, the residuals can be an order of magnitude greater.

3.2 Light curve creation

Since many of our fields are expected to be crowded, we used the *difference imaging analysis* technique to measure stellar fluxes, as implemented in the Difference Image Analysis Package `diapl2` (Wozniak 2000), which is an adaptation of the original algorithm outlined in Alard & Lupton (1998). The basic principle consists of subtracting a reference image

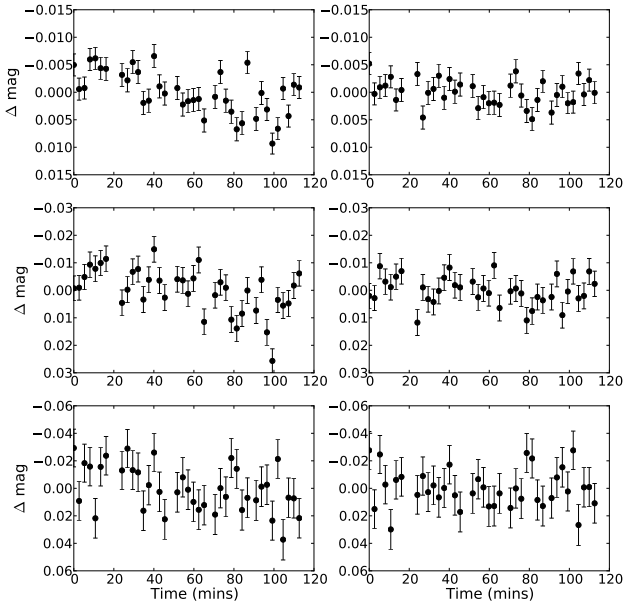

Figure 4. The results of applying the detrending algorithm for three light curves (from top to bottom having $g \sim 15.3$ mag, $g \sim 17.0$ mag, and $g \sim 18.8$ mag). Systematic trends that appear as large-scale wavelength-dependent effects tilting the light curves in the left panels are successfully corrected for as shown in the right panels.

from each science frame, after this reference image is degraded with a convolution kernel (a matrix used to smooth the seeing of the reference image) to match the seeing of each individual image. There are known to be mild variations in the Point Spread Function (PSF) of stars across the detector (Kuijken 2011). To account for this potential variation, we split each image into halves before applying the difference imaging algorithm (splitting the images into smaller units, such as eighths, causes the pipeline to fail in finding suitable stars to create a model PSF in the case of some subframes). An example of a reference subframe and the corresponding difference subframe obtained as the result of subtraction are illustrated in Figure 3 (Field OW_88D_15a, Chip #65).

Afterwards, the flux of 'residuals' on the subtracted images is measured through aperture photometry. These residuals are then added to the flux previously measured on the reference image. Thus, we obtain one photometric point for each star per image. Light curves which had less than ten photometric points were filtered out at this stage. Ultimately, the mean values of the measured instrumental magnitudes are calibrated using the AAVSO Photometric All-Sky Survey catalogue (APASS, Henden et al. 2009) for reference. Thus, all magnitude values listed in this paper are expressed using the Vega system.

The light curves were then corrected for systematic effects in the data using the `SYSREM` algorithm (Tamuz et al. 2005), which assumes that systematic trends affect measurements in a manner analogous to the effects of atmospheric extinction (dependent on the colour of each star and airmass of each image). The algorithm minimises the global expression:

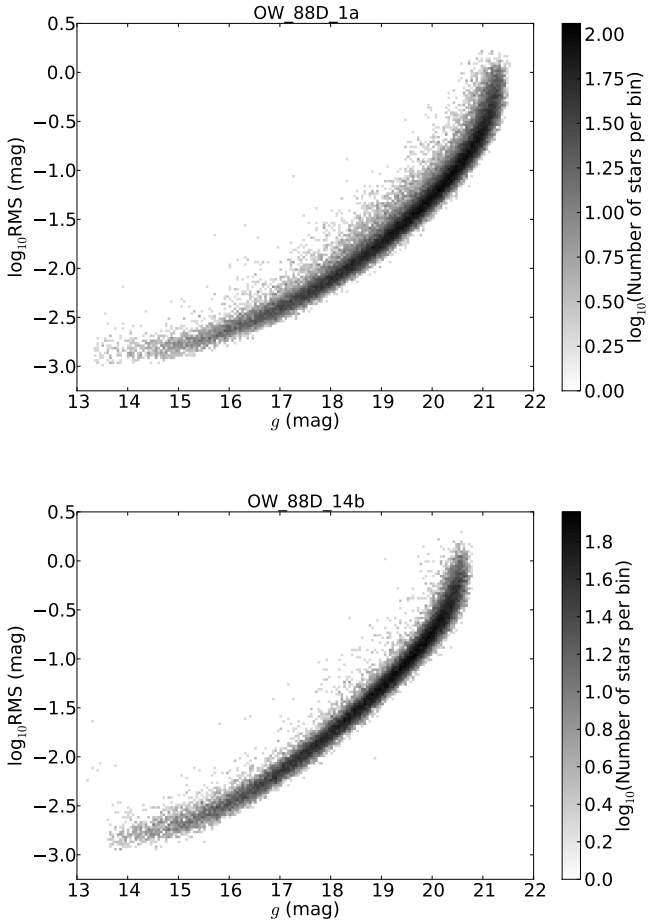

Figure 5. Distributions of standard deviations of magnitude for each light curve as a function of measured g-band magnitude, obtained using data from two fields observed during semester 88. The grey scale represents a 2D histogram showing the number of stars in bins of 0.05 × 0.025 mags.

$$S^2 = \sum_{ij} \frac{(r_{ij} - c_i a_j)^2}{\sigma_{ij}^2}, \quad (1)$$

where r_{ij} is the residual value of magnitude for each data point, c_i is the colour term for each star i, a_j is the airmass for each image j and σ_{ij} is the error. Basically, `SYSREM` subtracts the product $c_i a_j$ from the magnitude of each data point (see Tamuz et al. 2005; Barclay et al. 2011, for details). In Figure 4, we show non-detrended (left panels) and detrended (right panels) light curves for three non-variable stars, selected from the same field, OW_88D_13a. Their magnitudes are $g \sim 15.3$ mag, $g \sim 17.0$ mag, and $g \sim 18.8$ mag. As shown in Figure 4, `SYSREM` is able to successfully remove large-scale trends (appearing as tilts in the light curve). These trends are typically the result of atmospheric extinction effects, and are therefore wavelength-dependent.

To assess the quality of our photometric measurements, we study the distribution of the standard deviation from the mean of measured g-band magnitude, for each light curve on a field-by-field and chip-by-chip base. In Figure 5 we show examples of such plots for two fields, namely, OW_88D_1a and OW_88D_14b. The RMS plots for almost all of the fields from semester 88 look similar, as expected. However, excep-

Table 4. Results of flagging stars in Field OW_P88_1a.
Flag 1 = stars close to edge of images within 30 pixels
Flag 2 = saturated and faint stars ($g < 13.5$ mag and $g > 21.5$ mag resp.)
Flag 3 = stars with high sky background (1.5σ above median)

	No. Stars	%
Initial	60223	100
Flag 1	1926	3.2
Flag 2	3221	5.4
Flag 3	2274	3.8
All flags	7191	11.9
Unflagged	53032	88.1

tions are noticed in the case of two particular fields, namely OW_88D_6a and OW_88D_6b, which both show a higher RMS scattering over the entire distribution which we attribute to poor observing conditions (variable seeing and thick clouds were present during the observation run).

3.3 Flagging method for poor photometry detections

In order to investigate the number of bona fide variable stars, some of the automatically selected sources were manually checked through visual inspection of their light curves, their Discrete Fourier Transform (DFT) power spectra and the corresponding CCD images. As a result of this verification stage, we found that the light curves of many of our detections are affected by poor photometry. In most cases they were wrongly identified as variable stars since they were either within a few arcseconds of very bright objects, or situated in the diffraction spikes of saturated stars. We therefore modified our pipeline to identify three types of possible poor photometry objects. Firstly, we flagged stars located within 30 pixels to the edge of images, or close to bad columns of pixels. Secondly, we flagged very faint stars with low signal-to-noise ratio ($g > 21.5$ mag) and very bright stars which could be saturated ($g < 13.5$ mag). Finally, stars with a high background sky were flagged, including the faint sources on diffraction spikes of bright stars. The flagging threshold was set to a value of 1.5σ above the sky background median for the entire image.

In Table 4, we note the total number of stars in Field 1a and the number of stars which were flagged for one or more of the three reasons. For example, a very faint star with magnitude $g > 21.5$ mag and which is close to diffraction spikes would have been flagged twice. In total, 11.9 per cent of the stars in Field 1a were flagged.

3.4 Variability

We applied a variety of statistical tests to the light curves using the VARTOOLS Light Curve Analysis Program. As outlined by Graham et al. (2013) and Ramsay et al. (2014), different tests are better suited to identifying particular types of variable stars. For example, the Lomb Scargle test (LS, Lomb 1976; Scargle 1982) is suitable for finding short-period pulsating sources in irregularly spaced data, whilst the alarm test (Tamuz et al. 2006) and Analysis of Variance periodogram (Schwarzenberg-Czerny 1989) are ideal for finding eclipsing binaries and flare stars. Additionally, the Stetson J statistic (Stetson 1996), which was designed to find Cepheid variables, is optimally suited to detect high amplitude variables (e.g. contact binaries, flares and long period pulsators).

Since our main goal is to identify short-period ($P_{orb} <$ 60 min) variable stars, we use the LS periodogram as our main tool. The mean cadence of our observations is 3.2 min, while the median cadence is 2.7 min. Therefore, we chose to set our short period limit to 6.0 min (which corresponds to the Nyquist frequency, also see Figure 2), and set the long period limit to 2.2 hrs (corresponding to the duration of the observations).

For each light curve we identify the period and the false alarm probability (FAP) corresponding to the most statistically significant peak in the power spectrum. FAP is a statistic which describes the probability that the highest peak is caused by random noise. In Figures 6a and 6b we show the distribution of all measured stars in period - $\log_{10}$(FAP) space, where the period represents the highest peak in the power spectrum of individual light curves. The more negative the value of $\log_{10}$(FAP), the higher the probability that the light curve shows real variability on that time-scale. In theory, a star having $\log_{10}(\mathrm{FAP}) = -2.5$ has a probability of being a variable object at the 3σ confidence level. The vast majority of sources are located in the upper part of figure, meaning that (as expected) most stars are not detected as variable using our methods. Only 0.51 per cent of the $1.6{\times}10^6$ sources from semester 88 have $\log_{10}(\mathrm{FAP}) < -2.5$, i.e. are detected as variable within the 3σ confidence interval.

However, in the case of real data, the threshold for variability can be more negative than the theoretical value $\log_{10}(\mathrm{FAP}) = -2.5$, because of systematic effects such as red noise. This can be seen in Figure 6, where there is a greater spread in $\log_{10}$(FAP) values towards longer periods. This indicates the presence of red noise, which affects the stars with possible variability on longer time-scale. Thus, we use the median absolute deviation from the median (MAD), a more robust statistic to detect the variable candidates which are outliers (in the very long tail of the distribution).

We apply the same procedure and codes explained in detail by Barclay et al. (2011) and Ramsay et al. (2014). We sort the data according to period and group them in bins of 2 minutes. For all stars in each bin, we then compute the median of $\log_{10}$(FAP) values ($median_{LogFAP}$), and the median absolute deviation from $median_{LogFAP}$ (MAD_{LogFAP}), and select as variable candidates the stars which obey the condition:

$$\log_{10}(FAP) < median_{LogFAP} + (n \times MAD_{LogFAP}) \qquad (2)$$

where n is an integer which defines how far a source is from the local median ($median_{LogFAP}$). Since there is no pre-established recipe, the stars are selected by experimenting with different values of n.

An example of this experiment is shown in Figure 6a. We overlay the automatically detected variable stars from Field 1a, on top of all stars measured in semester 88. The number of stars selected for each value of n are listed in the legend. As the same stars that were selected for high values of n are also included in the lower n value sets, for clarity in Figure 6a we plot each star only once. We notice

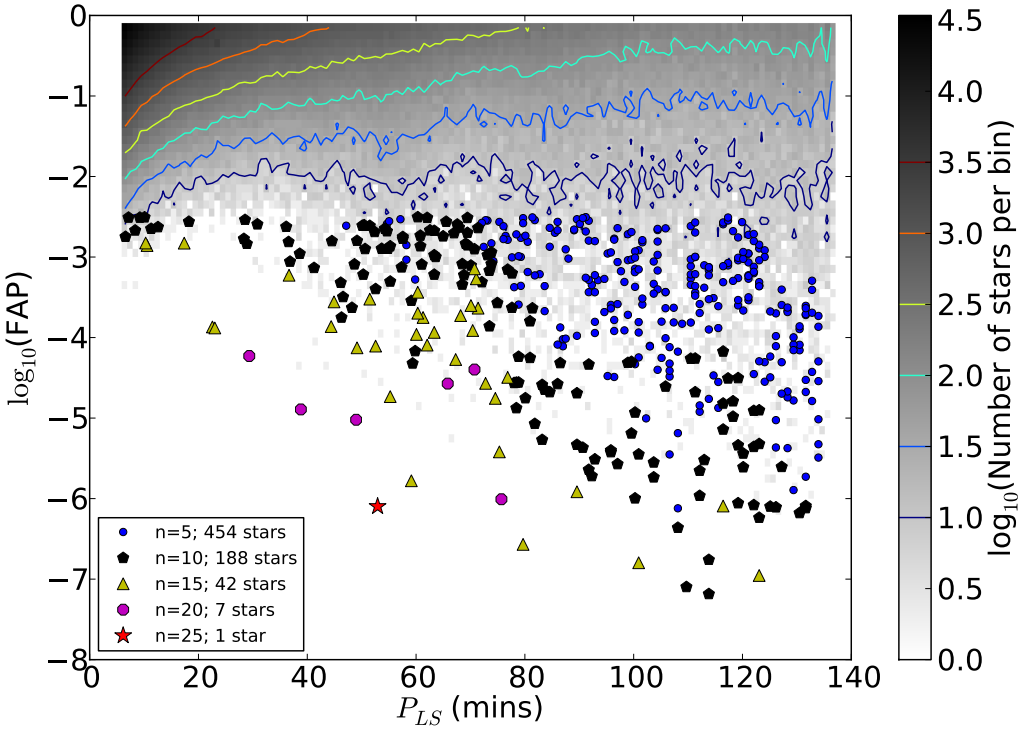

(a) Variable stars in Field OW_88D_1a.

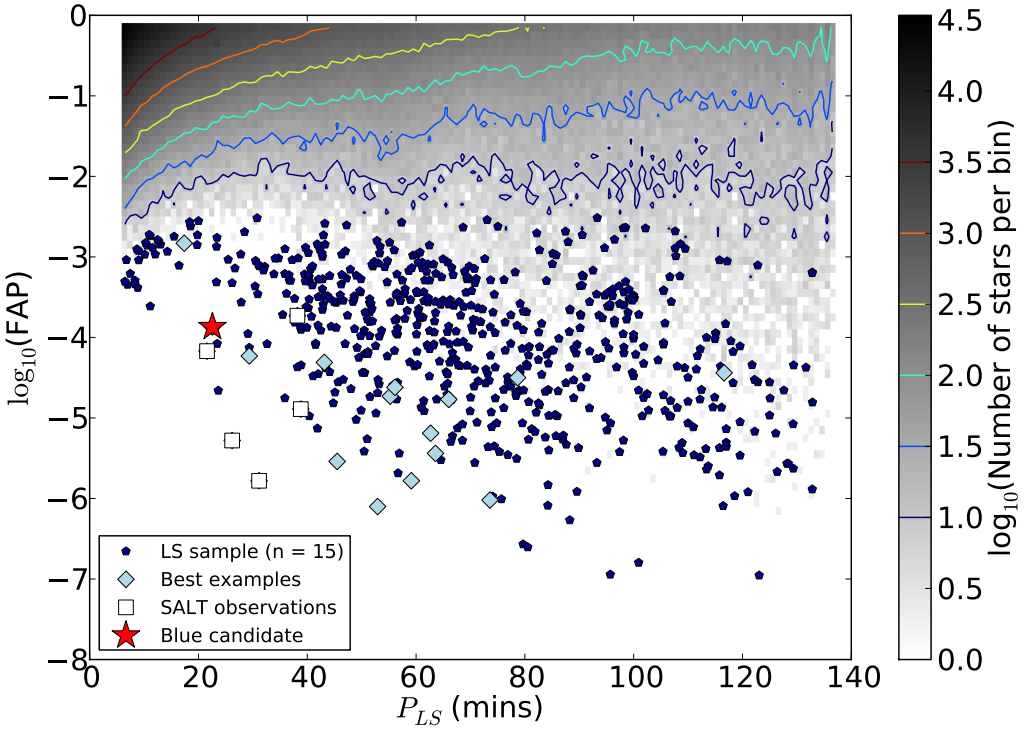

(b) Variable stars in ESO semester 88.

Figure 6. Distribution of all 1.4×10^6 unflagged stars from semester 88 data in Period - $\log_{10}$(FAP) space. Data are grouped in 1-minute bins on the period axis and in 0.1 units on the $\log_{10}$(FAP) axis. Coloured contours are plotted starting from $\log_{10}$(number of stars) = 1 and then at levels incremented by 0.5 to indicate trends in the distribution. In Figure 6a the number of variable candidates automatically selected from Field 1a data are plotted on top. In Figure 6b the variable candidates are overlaid.

Table 5. The variable candidates automatically selected from the entire set of data observed during ESO semester 88, for a set of values of n are listed. The selection algorithm was applied on the set of unflagged stars.

Period	0-20 min	20-40 min	P > 40 min	Total
n	(No. stars)	(No. stars)	(No. stars)	(No. stars)
5	177	139	4546	4862
10	177	136	2017	2330
15	29	56	528	613
20	0	18	126	144
25	0	6	29	35

that the value of n and the number of selected stars are inversely proportional. This proves that the lower the value of n, the higher the probability that the selected stars are poor photometry detections because their light curves show variations caused by systematic effects.

We show our sample of variable candidates automatically selected using MAD statistic of LS false alarm probability in Table 5. The total number of automatically selected candidates for a set of values of n are shown in the last column, 'Total'. Furthermore, we group the stars in intervals of periods associated with the three AM CVn states (based on disc and outbursting properties). We have chosen the set of variable stars detected for $n = 15$ in the next steps of data analysis.

3.5 Colour Analysis

The VPHAS+ survey (Drew et al. 2014) obtains photometric measurements in u-, g-, r-, i- and Hα-bands along the southern Galactic plane. Using these multi-band colours, we can identify specific types of variable stars which lie within certain regions of colour-colour space. As an example, AM CVn systems are known to be very blue sources and thus occupy a distinctive region of the $u - g$ vs $g - r$ colour plane (Carter et al. 2013). We have additionally cross-matched our data with other multi-colour survey catalogues such as the Two Micron All Sky Survey (2MASS, Jarrett et al. 2000) and the AAVSO Photometric All-Sky Survey (APASS, Henden et al. 2009). However, these surveys do not reach the depths of OmegaWhite, and thus some of our fainter sources currently lack colour information from these surveys.

Although we found that 98 per cent of the stars in Field 1a match stars in four VPHAS+ fields, some of our fields lack colour information because they have not yet been fully covered by the VPHAS+ survey. Out of the 26 deg^2 of data observed in semester 88, 7 deg^2 (i.e. 26.9 per cent of our fields, namely Fields 4b, 5a, 5b, 8a, 8b, 9a, 9b) lack colour data. Thus, in the case of our sample of 613 variable candidates selected for $n = 15$ (see Section 3.4), we found information in all three u, g, r bands for 362 stars (59.1 per cent). We show their distribution in colour - colour space in Figure 7, and list their properties in Table A2 .

4 INITIAL SURVEY RESULTS

We have extracted the light curves of 1.6×10^6 stars from the initial 26 square degrees of the OmegaWhite Survey (semester 88 data). Of these stars, 2.0×10^5 (12.5 per cent) were flagged in the manner described in Section 3.3. Variable candidates were selected from the 1.4 $\times10^6$ unflagged stars remaining (87.5 per cent), using the automatic method described in Section 3.4. We thus identified a subset of 613 sources that were significantly variable (with $\log_{10}$(FAP) < -2.5) using $n = 15$ in our MAD routines, and list their properties in Table A2. Of these, 29 sources exhibit dominant periods less than 20 minutes (4.7 per cent), 56 sources have periods between 20 minutes and 40 minutes (9.1 per cent), and 528 sources have periods greater than 40 minutes (86.2 per cent).

Furthermore, a subsample of 20 variable stars with both colour indices available has been selected as the most significant examples, after inspecting the light curves, DFT power spectra, and CCD reference images of each source. They were selected from the sample for $n = 20$, and from the 29 stars selected for $n = 15$ for periods smaller than 20 minutes. The individual light curves of these examples are displayed in Figure 8 and their properties are listed in Table 6. Only the first star shows sinusoidal modulations on a period smaller than 20 minutes, seven have periods between 20 - 40 minutes, and the rest exhibit variations on longer periods.

In Figure 7, we show the colour indices of 1.1 $\times10^6$ unflagged colour-matched stars in the $u - g$ vs $g - r$ plane. We overlay the colours of the 362 variable candidates which show colour information and for comparison plot 14 of the known AM CVn stars identified in SDSS data (Carter et al. 2013), as well as the four known detached double white dwarf systems with periods less than 1 hour (Kilic et al. 2011; Hermes et al. 2012; Kilic et al. 2014). One of the 362 variables, namely OW J074106.1–294811.2 ($g - r = -0.08$ and $u - g = -1.25$) has colours consistent with those of an AM CVn star, a short-period double-detached system, or a pulsating white-dwarf/subdwarf candidate (as shown in Figure 7 and in Table 6). We present follow-up spectral observations of this source, and discuss its possible nature in Section 4.1.

The majority of the 613 variable candidates exhibit periodic variations, amplitudes or colours that are more consistent with pulsating sources, and are likely to be either δ Sct stars, SX Phe pulsators or pulsating white dwarfs. We have also detected longer period systems, such as contact binary candidates. An example of such a system with $P_{LS} \gtrsim 116$ min is shown in Figure 8.

4.1 Follow-up Spectroscopic Observations

We have so far obtained identification spectroscopy for six variable candidates (OW J080916.7–292158.0, OW J075359.8–275732.6, OW J075532.6–280854.3, OW J074513.2–261036.0, OW J074106.4–293325.5, and OW J074106.1–294811.0) using the 10-m Southern African Large Telescope (Buckley et al. 2006) between December 2014 and April 2015. These variables were selected for follow-up observations as they were some of our most likely UCB candidates: they exhibited relatively fast variations with low $\log_{10}$(FAP) values (see Figure 6a), and are some

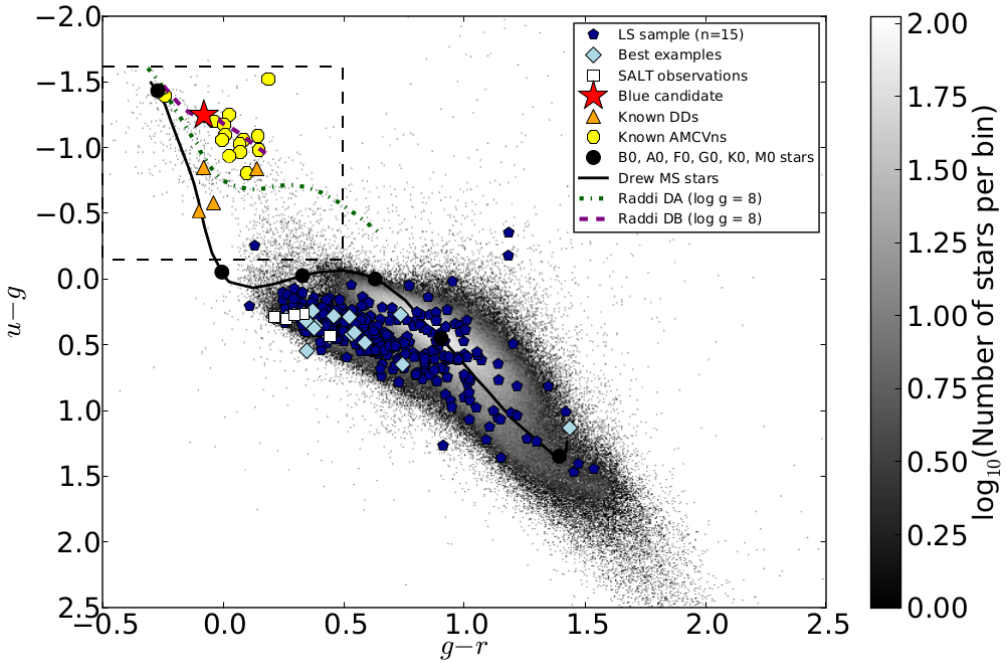

(a) colour-colour plot of all fields observed during semester 88

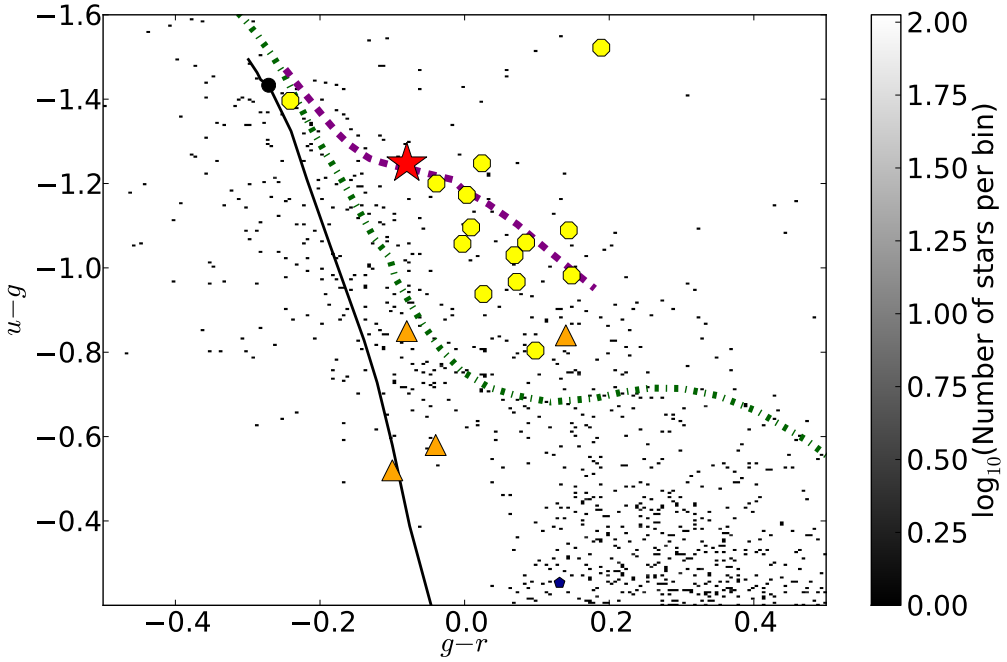

(b) Zoom in of the blue region

Figure 7. Distribution of all stars measured in semester 88 data, for which VPHAS+ colour information was available is shown in $u-g$ vs $g-r$ space. In the upper panel, stars are distributed in a 2D histogram with bins of 0.005 mag units. The sample of variable candidates selected for $n = 15$ are overlaid. Of the 613 variable candidates, only 362 have both colour indices and thus could be represented. For comparison, we plot 14 of the known AM CVn stars identified in SDSS data as circles (Carter et al. 2013), and the four known detached double white dwarf systems with periods less than 1 hour as triangles (Kilic et al. 2011; Hermes et al. 2012; Kilic et al. 2014). We also plot tracks for main sequence stars, DA and DB white dwarfs. For the MS track, we used the synthetic colours provided by Drew et al. (2014) for R_v=3.1 and extinction coefficient $A_0 = 0$. The synthetic colours for the cooling tracks were taken from Raddi et al. (in prep, private communication) for models with a surface gravity of $\log g = 8.0$. A close-up of the blue-square (i.e. the square where all the blue UCBs are expected to be found) is shown in the bottom panel. One of our variable sources, OW J074106.1–294811.0, lies in this blue region together with other known AM CVn stars.

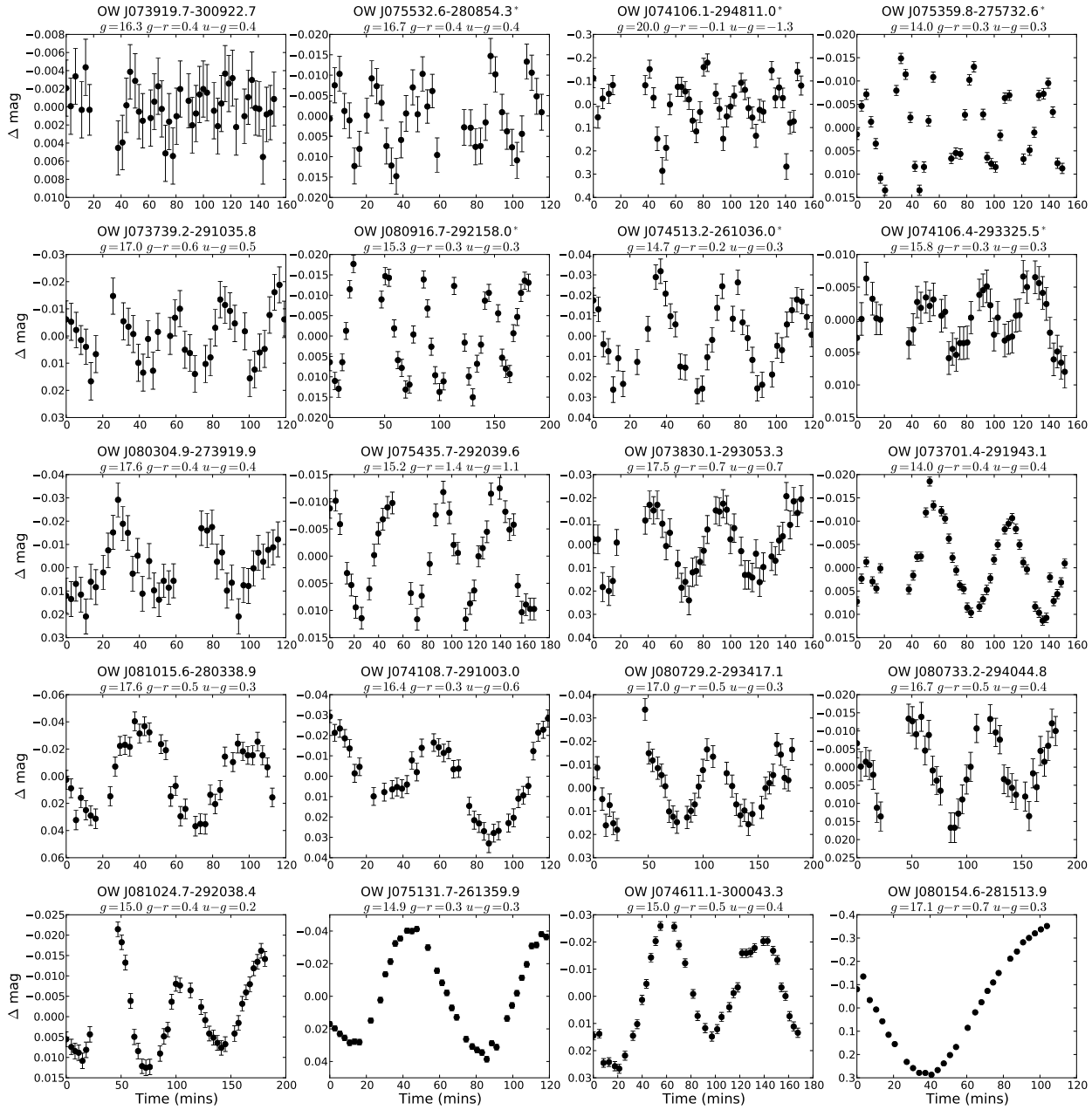

Figure 8. Example set of light curves selected from 613 variable candidates detected in semester 88 data. The six stars marked with an asterisk have been followed-up spectroscopically using the RSS spectrograph on SALT.

of the bluest sources of our 362 variable candidates. Of these targets, OW J074106.1–294811.2 is the only target to exhibit colours consistent with AM CVn systems, as shown in Figure 7).

Three exposures of 180 s each were obtained for five of the brighter targets (as listed in Table 7) using the Robert Stobie Spectrograph (RSS, Kobulnicky et al. 2003) in long-slit mode, with a 1.5″ slit and the PG0300 grating (providing a dispersion of 3.04 Å per binned pixel and a wavelength range of ∼3200 - 9000 Å). For our faint blue target OW J074106.1–294811.0, we obtained a set of two exposures of 1200 s each over two nights (for a total of four 1200s exposures). Spectra were reduced using standard IRAF (Tody 1986, 1993) and PYSALT (Crawford et al. 2010) routines, with either an Ar arc or a Xe arc for wavelength calibration. The resulting spectral resolution was ∼4 Å for the mean combined spectrum of each source.

The spectra for each of the five brighter variables appear to be similar; they all exhibit strong Balmer absorption lines with some evidence of weaker Na I and Mg I lines. In order to identify the spectral type, we measured the equivalent width (EW) ratio of the Na I doublet (5896 Å, 5890 Å) to Hα for each variable, and compared these values with the EW ratios measured in various spectral types from model `Atlas9` data (Castelli & Kurucz 2004). In Figure 9, we overlay our variable EW ratios on the measured EW ratios for several spectral types (fitted by an exponential curve). Hence, we can deduce that our variables observed using SALT are most

Table 6. Parameters of the variable stars shown in Figure 8: star ID; RA and Dec; Lomb Scargle period (P_{LS}) and false alarm probability ($\log_{10}$(FAP)) of the highest peak in the periodogram, OW calibrated g-band magnitude, RMS of magnitude, VPHAS+ colour indices $g-r$ and $u-g$, and comments on variability type.

Star ID	RA (J2000) (hh:mm:ss)	DEC (J2000) (°:′:″)	P_{LS} (min)	$\log_{10}$(FAP)	OWg (mag)	RMS (mag)	$g-r$ (mag)	$u-g$ (mag)	Comments
OW J073919.7–300922.7	07:39:19.7	–30:09:22.7	17.38	–2.83	16.26	0.002	0.38	0.37	
OW J075532.6–280854.3*	07:55:32.6	–28:08:54.3	21.57	–4.17	16.70	0.008	0.44	0.44	δ Sct (F5V)
OW J074106.1–294811.0*	07:41:06.1	–29:48:11.0	22.56	–3.87	20.02	0.106	–0.08	–1.25	pulsating subdwarf?
OW J075359.8–275732.6*	07:53:59.8	–27:57:32.6	26.19	–5.28	13.98	0.008	0.26	0.30	δ Sct (F2V)
OW J073739.2–291035.8	07:37:39.2	–29:10:35.8	29.34	–4.23	16.97	0.006	0.59	0.48	
OW J080916.7–292158.0*	08:09:16.7	–29:21:58.0	31.14	–5.78	15.30	0.010	0.29	0.27	δ Sct (F2V)
OW J074513.2–261036.0*	07:45:13.2	–26:10:36.0	38.19	–3.73	14.73	0.004	0.21	0.29	δ Sct (F0V)
OW J074106.4–293325.5*	07:41:06.4	–29:33:25.5	38.81	–4.89	15.75	0.004	0.33	0.27	δ Sct (F2V)
OW J080304.9–273919.9	08:03:04.9	–27:39:19.9	43.13	–4.31	17.61	0.012	0.38	0.36	
OW J075435.7–292039.6	07:54:35.7	–29:20:39.6	45.49	–5.54	15.23	0.008	1.44	1.13	
OW J073830.1–293053.3	07:38:30.1	–29:30:53.3	52.93	–6.10	17.47	0.012	0.74	0.65	
OW J073701.4–291943.1	07:37:01.4	–29:19:43.1	55.25	–4.73	14.02	0.007	0.38	0.37	
OW J081015.6–280338.9	08:10:15.6	–28:03:38.9	56.12	–4.62	17.62	0.021	0.52	0.29	
OW J074108.7–291003.0	07:41:08.7	–29:10:03.0	59.13	–5.78	16.41	0.012	0.35	0.55	
OW J080729.2–293417.1	08:07:29.2	–29:34:17.1	62.68	–5.19	17.00	0.012	0.46	0.28	
OW J080733.2–294044.8	08:07:33.2	–29:40:44.8	63.57	–5.44	16.71	0.009	0.53	0.42	
OW J081024.7–292038.4	08:10:24.7	–29:20:38.4	66.01	–4.77	15.04	0.009	0.37	0.24	
OW J075131.7–261359.9	07:51:31.7	–26:13:59.9	73.59	–6.02	14.89	0.027	0.34	0.32	
OW J074611.1–300043.3	07:46:11.1	–30:00:43.3	78.67	–4.50	15.01	0.012	0.54	0.41	
OW J080154.6–281513.9	08:01:54.6	–28:15:13.9	116.63	–4.44	17.11	0.210	0.74	0.27	Contact binary

*Observed spectroscopically with SALT, results presented in Section 4.1

Table 7. Approximate spectral type of SALT-observed variables

SALT-observed Variable	EW (Na I)	EW (Hα)	EW Ratio (Na I/Hα)	$\sim$ Spectral Type
OW J075532.6–280854.3	3.033 ± 0.082	15.599 ± 0.133	0.194 ± 0.028	F5V
OW J074106.4–293325.5	1.948 ± 0.030	14.443 ± 0.193	0.135 ± 0.020	F2V
OW J080916.7–292158.0	1.938 ± 0.019	15.971 ± 0.201	0.121 ± 0.016	F2V
OW J075359.8–275732.6	1.661 ± 0.022	15.775 ± 0.199	0.105 ± 0.018	F2V
OW J074513.2–261036.0	1.071 ± 0.008	16.297 ± 0.068	0.065 ± 0.066	F0V

likely to be late A-type or early F-type stars, and thus possible low-amplitude δ Sct.

Prior to acquiring SALT spectra, the target OW J074106.1–294811.0 was our most likely UCB candidate. This source is relatively faint ($g = 20.02$ mag) and the light curve shows sinusoidal modulations on a period of 22.6 minutes (see Figure 10 for the light curve and Discrete Fourier transform of this target). In the right panel of Figure 10, we show the SALT-observed spectrum of this target, along with two spectra from neighbouring stars for comparison. In the target spectra, there is weak evidence for the Balmer absorption lines Hβ and Hγ, but no Hα (either due to intrinsic weakness of the line, or (partial) infill by emission). Thus, this object is not likely to be a UCB (which would exhibit relatively strong helium emission and little to no hydrogen). Furthermore, the source is relatively blue which is consistent with the properties of a massive hot DA white dwarf. However, the absorption lines are relatively narrow, and thus it is unlikely that this is the case. The OmegaWhite g-band magnitude we observed is $g \approx 20.02$ mag, while it was recorded by VPHAS+, on two separate epochs, to have $g \approx 20.00$ mag and $g \approx 19.98$ mag respectively. This implies that the target is not likely to

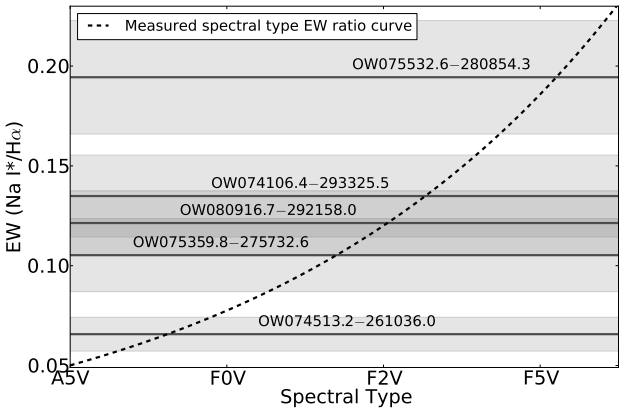

Figure 9. Equivalent Width ratios of Na I doublet (5896 Å, 5890 Å) to Hα for a range of spectral types. Measured EW ratios increase exponentially towards later spectral types (as shown by the dashed curved line). The measured EW ratio for each of the five SALT variables are shown by a line spanning all spectral types, with respective measurement uncertainties indicated by shading. Likely spectral classes for each SALT variable are listed in Table 7.

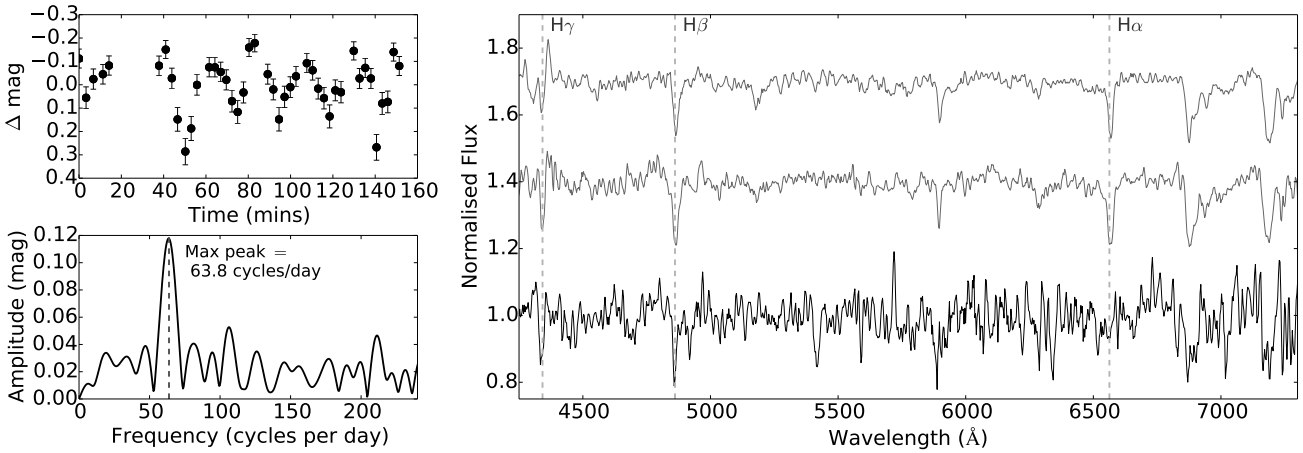

Figure 10. Properties of blue variable OW J074106.1–294811.0, including the OmegaWhite light curve (upper left panel), the Discrete Fourier Transform power spectrum (lower left panel), and the SALT-observed spectrum (right panel). We plot the continuum-normalised spectra of the target (lower black spectrum) and the spectra of two neighbouring stars for comparison (two upper grey spectra). All spectra have been smoothed by a running average of 3 and an offset has been applied for visualisation purposes.

be a cataclysmic variable in outburst, where the variations may be due to strong quasi-periodic oscillations (QPOs, see Morales-Rueda & Marsh (2002) for examples of outbursting CVs). Although very rare, this does not rule out that the variations may be due to QPOs during quiescence (for e.g. RAT J1953+1859 exhibits high amplitude QPOs during quiescence (Ramsay et al. 2009)). Since it is a very blue source, it is possibly a pulsating subdwarf, although with a relatively long pulsation period. Dedicated high speed photometry of this object should reveal if this object is indeed a pulsator.

5 DISCUSSION AND SUMMARY

The initial 26 square degrees of OmegaWhite data have been fully processed and the light curves of $1.6{\times}10^6$ stars have been extracted. Of these stars, 12.5 per cent were flagged as having light curves which could have been degraded by various effects, and were thus disregarded when identifying variable candidates using the verification methods described in Section 3.4. We find that 0.4 per cent of the stars in semester 88 satisfy our selection criteria: they are not flagged as poor photometry detections, their Lomb Scargle periods are between 5 min and 120 min, their $\log_{10}(\mathrm{FAP}) < -2.5$, and they were selected using a MAD n value $\geqslant 15$. Furthermore, we find that more than 80 per cent (the majority) of the 613 sources identified as variables through our pipeline (using n = 15) have $\mathrm{P}_{LS} > 40$ min, whereas less than 8 per cent of our variables have $\mathrm{P}_{LS} < 20$ min.

In Table 6 and Figure 8, we show the properties of 20 relatively blue sources as examples of light curves from our 613 variable candidates. The light curves of 19 of these variables each exhibit variations on a dominant period between 22 min and 80 min. We are also able to detect relatively longer period systems, as illustrated by the contact binary candidate (shown in Figure 8).

Using spectral identification, we determined that at least five of the short-period variable candidates are likely to be low-amplitude δ Sct type stars. The remaining 608 variable candidates, including fourteen of the example variables from Table 6, have not yet been identified with spectroscopy. Some of these variables occupy a similar region of the colour-colour space to our five δ Sct candidates (as shown in Figure 7), and also exhibit fast modulations with periods between 17 min and 80 min. In addition to more detailed analysis of the photometry of these systems, spectroscopy is now needed to determine whether the majority are either low-amplitude δ Sct stars, SX Phe pulsators or pulsating white dwarfs.

Within the initial 26 square degrees of OmegaWhite, only one of our 613 candidate variables exhibit the very blue colours consistent with AM CVn systems (Carter et al. 2013). However, as it exhibits Balmer absorption lines in its spectrum, it is unlikely to be an UCB. As it is a very blue source, with weak thin hydrogen lines, it is more likely to be a pulsating subdwarf star. Although we have not discovered any AM CVn within the initial 26 square degrees, this is a small fraction of our expected coverage and is thus consistent with recent AM CVn space density estimates (Carter et al. 2013). Using these estimates, we expect less than one AM CVn within the initial 26 square degrees. In a future OmegaWhite paper that will examine ∼150 square degrees of the Galactic Plane, we plan to make detailed simulations of the expected AM CVn space densities as a function of Galactic latitude.

Now that we have formalised our verification procedure and analysed the initial results, we will apply these techniques to future OmegaWhite data. So far 148 square degrees of OmegaWhite data has been observed, and we have been allocated an additional 64 square degrees (see Section 2 for details). This will allow us to get a better understanding of the space density of sources such as UCBs and δ Sct along the Galactic plane, as well as within the Galactic Bulge. Furthermore, we are planning photometric and spectroscopic follow-up campaigns for variable candidates, which is essential for their precise classification.

6 ACKNOWLEDGEMENTS

The authors gratefully acknowledge funding from the Erasmus Mundus Programme SAPIENT, the National Research Foundation of South Africa (NRF), the Nederlandse Organisatie voor Wetenschappelijk Onderzoek (the Dutch Organisation for Science Research), Radboud University and the University of Cape Town. The ESO observations used in this paper are based on observations made with ESO Telescopes at the La Silla Paranal Observatory under programme IDs: 088.D-4010(B), 090.D-0703(A), 090.D-0703(B), 091.D-0716(A), 091.D-0716(B), 092.D-0853(B), 093.D-0937(A), 093.D-0753(A), 094.D-0502(A), 094.D-0502(B), and 177.D-3023 (VPHAS+). Some of the observations reported in this paper were obtained with the Southern African Large Telescope (SALT) under program 2014-2-SCI-030 (PI: Sally Macfarlane). Furthermore, we thank the anonymous referee for the useful comments which have helped to improve the paper.

REFERENCES

Alard C., Lupton R. H., 1998, ApJ, 503, 325
Amaro-Seoane P., et al., 2013, GW Notes, Vol. 6, p. 4-110, 6, 4
Barclay T., Ramsay G., Hakala P., Napiwotzki R., Nelemans G., Potter S., Todd I., 2011, MNRAS, 413, 2696
Becker A. C., et al., 2004, ApJ, 611, 418
Borucki W. J., et al., 2010, Science, 327, 977
Breger M., 1979, PASP, 91, 5
Breger M., 2000, in Breger M., Montgomery M., eds, Delta Scuti and Related Stars Vol. 210 of Astronomical Society of the Pacific Conference Series, δ Scuti stars (Review). p. 3
Buckley D. A. H., Swart G. P., Meiring J. G., 2006, in Society of Photo-Optical Instrumentation Engineers (SPIE) Conference Series Vol. 6267 of Society of Photo-Optical Instrumentation Engineers (SPIE) Conference Series, Completion and commissioning of the Southern African Large Telescope. p. 0
Capaccioli M., Schipani P., 2011, The Messenger, 146, 2
Carter P. J., et al., 2013, MNRAS, 429, 2143
Castelli F., Kurucz R. L., 2004, ArXiv Astrophysics e-prints
Chang S.-W., Protopapas P., Kim D.-W., Byun Y.-I., 2013, AJ, 145, 132
Crawford S. M., et al., 2010, in Society of Photo-Optical Instrumentation Engineers (SPIE) Conference Series Vol. 7737 of Society of Photo-Optical Instrumentation Engineers (SPIE) Conference Series, PySALT: the SALT science pipeline. p. 25
Drake A. J., et al., 2009, ApJ, 696, 870
Drew J. E., et al., 2014, MNRAS, 440, 2036
Graham M. J., Drake A. J., Djorgovski S. G., Mahabal A. A., Donalek C., Duan V., Maker A., 2013, MNRAS, 434, 3423
Groot P. J., et al., 2003, MNRAS, 339, 427
Hartman J. D., Gaudi B. S., Holman M. J., McLeod B. A., Stanek K. Z., Barranco J. A., Pinsonneault M. H., Kalirai J. S., 2008, ApJ, 675, 1254
Henden A. A., Welch D. L., Terrell D., Levine S. E., 2009, in American Astronomical Society Meeting Abstracts 214 Vol. 214 of American Astronomical Society Meeting Abstracts, The AAVSO Photometric All-Sky Survey (APASS). p. 407.02
Hermes J. J., et al., 2012, ApJ, 757, L21
Israel G. L., Panzera M. R., Campana S., Lazzati D., Covino S., Tagliaferri G., Stella L., 1999, A&A, 349, L1
Jarrett T. H., Chester T., Cutri R., Schneider S., Skrutskie M., Huchra J. P., 2000, AJ, 119, 2498
Jonker P. G., et al., 2011, ApJS, 194, 18
Kilic M., Brown W. R., Gianninas A., Hermes J. J., Allende Prieto C., Kenyon S. J., 2014, ArXiv e-prints
Kilic M., Brown W. R., Hermes J. J., Allende Prieto C., Kenyon S. J., Winget D. E., Winget K. I., 2011, MNRAS, 418, L157
Kim D.-W., et al., 2010, AJ, 139, 757
Kobulnicky H. A., Nordsieck K. H., Burgh E. B., Smith M. P., Percival J. W., Williams T. B., O'Donoghue D., 2003, in Iye M., Moorwood A. F. M., eds, Instrument Design and Performance for Optical/Infrared Ground-based Telescopes Vol. 4841 of Society of Photo-Optical Instrumentation Engineers (SPIE) Conference Series, Prime focus imaging spectrograph for the Southern African large telescope: operational modes. pp 1634–1644
Kuijken K., 2011, The Messenger, 146, 8
Lang D., Hogg D. W., Mierle K., Blanton M., Roweis S., 2010, AJ, 139, 1782
Law N. M., et al., 2009, PASP, 121, 1395
Levitan D., et al., 2011, ApJ, 739, 68
Levitan D., Groot P. J., Prince T. A., Kulkarni S. R., Laher R., Ofek E. O., Sesar B., Surace J., 2015, MNRAS, 446, 391
Lomb N. R., 1976, Ap&SS, 39, 447
McNamara D. H., Clementini G., Marconi M., 2007, AJ, 133, 2752
Morales-Rueda L., Groot P. J., Augusteijn T., Nelemans G., Vreeswijk P. M., van den Besselaar E. J. M., 2006, MNRAS, 371, 1681
Morales-Rueda L., Marsh T. R., 2002, MNRAS, 332, 814
Nelemans G., Portegies Zwart S. F., Verbunt F., Yungelson L. R., 2001, A&A, 368, 939
Petersen J. O., Christensen-Dalsgaard J., 1999, A&A, 352, 547
Pollacco D., et al., 2006, Ap&SS, 304, 253
Ramsay G., et al., 2009, MNRAS, 398, 1333
Ramsay G., et al., 2014, MNRAS, 437, 132
Ramsay G., Hakala P., 2005, MNRAS, 360, 314
Ramsay G., Hakala P., Cropper M., 2002, MNRAS, 332, L7
Ramsay G., Napiwotzki R., Hakala P., Lehto H., 2006, MNRAS, 371, 957
Rappaport S., Joss P. C., Webbink R. F., 1982, ApJ, 254, 616
Rau A., Roelofs G. H. A., Groot P. J., Marsh T. R., Nelemans G., Steeghs D., Salvato M., Kasliwal M. M., 2010, ApJ, 708, 456
Rodríguez E., López-González M. J., 2000, A&A, 359, 597
Roelofs G. H. A., et al., 2009, MNRAS, 394, 367
Roelofs G. H. A., Groot P. J., Nelemans G., Marsh T. R., Steeghs D., 2006, MNRAS, 371, 1231
Roelofs G. H. A., Nelemans G., Groot P. J., 2007, MNRAS, 382, 685
Scargle J. D., 1982, ApJ, 263, 835

Schwarzenberg-Czerny A., 1989, MNRAS, 241, 153
Smak J., 1967, Information Bulletin on Variable Stars, 182, 1
Solheim J.-E., 2010, PASP, 122, 1133
Stetson P. B., 1996, PASP, 108, 851
Tamuz O., Mazeh T., North P., 2006, MNRAS, 367, 1521
Tamuz O., Mazeh T., Zucker S., 2005, MNRAS, 356, 1466
Tody D., 1986, in Crawford D. L., ed., Instrumentation in astronomy VI Vol. 627 of Society of Photo-Optical Instrumentation Engineers (SPIE) Conference Series, The IRAF Data Reduction and Analysis System. p. 733
Tody D., 1993, in Hanisch R. J., Brissenden R. J. V., Barnes J., eds, Astronomical Data Analysis Software and Systems II Vol. 52 of Astronomical Society of the Pacific Conference Series, IRAF in the Nineties. p. 173
Wagner R. M., et al., 2014, The Astronomer's Telegram, 6669, 1
Warner B., Robinson E. L., 1972, MNRAS, 159, 101
Warner B., Woudt P. A., 2002, PASP, 114, 129
Wozniak P. R., 2000, Acta Astron., 50, 421

APPENDIX A: OMEGAWHITE SEMESTER 88 FIELD COORDINATES AND VARIABLE CANDIDATES

Table A1. We note the sky co-ordinates for the center of all semester 88 fields together with the number of light curves for sources which lie in the range 13.5 mag $< g <$ 21.5 mag.

Field ID	RA (J2000)	DEC (J2000)	Number of Light Curves
1a	07:38:57.9	–29:39:20.1	57002
1b	07:43:34.0	–29:39:15.8	62116
2a	07:48:15.9	–29:39:20.1	54741
2b	07:52:52.1	–29:39:15.9	59465
3a	07:57:33.9	–29:39:20.1	49846
3b	08:02:10.0	–29:39:15.9	56663
4a	08:06:51.9	–29:39:20.1	64465
4b	08:11:28.1	–29:39:15.9	61218
5a	08:16:09.2	–29:39:19.9	57718
5b	08:20:45.3	–29:39:16.1	56695
6a	07:43:31.2	–28:39:17.1	57812
6b	07:48:05.3	–28:39:12.9	49519
8a	08:01:56.8	–28:39:17.0	54573
8b	08:06:30.3	–28:39:13.0	61541
9a	08:11:09.3	–28:39:17.0	61184
9b	08:15:42.7	–28:39:13.0	54986
11a	07:48:02.9	–27:39:09.1	48046
11b	07:52:33.9	–27:39:05.0	55484
12a	07:57:10.3	–27:39:09.0	60343
12b	08:01:41.2	–27:39:05.0	67633
13a	08:06:17.8	–27:39:09.0	60572
13b	08:10:48.8	–27:39:05.0	55318
14a	07:38:54.2	–26:38:54.1	35784
14b	07:43:22.7	–26:38:49.9	40929
15a	07:52:28.2	–26:38:54.1	62493
15b	07:56:56.7	–26:38:50.0	55150

Table A2. Parameters of the 613 variable candidates (selected using $n = 15$): star ID; RA and Dec; Lomb Scargle period (P_{LS}) and false alarm probability ($\log_{10}$(FAP)) of the highest peak in the periodogram, OW calibrated g-band magnitude, RMS of magnitude, VPHAS+ colour indices $g - r$ and $u - g$, and comments on variability type.

Star ID	RA (J2000) (hh:mm:ss)	DEC (J2000) (°:′:″)	P_{LS} (min)	$\log_{10}$(FAP)	OWg (mag)	RMS (mag)	$g - r$ (mag)	$u - g$ (mag)
OW J081124.34–295822.8	08:11:24.34	–29:58:22.8	6.47	–3.31	18.04	0.033		
OW J080916.81–281226.2	08:09:16.81	–28:12:26.2	6.75	–3.04	18.13	0.008	0.83	0.55
OW J075449.27–263259.3	07:54:49.27	–26:32:59.3	6.98	–3.34	20.50	0.087	1.17	
OW J075833.40–270202.5	07:58:33.40	–27:02:02.5	7.46	–3.21	20.61	0.110	1.13	
OW J074809.65–291214.1	07:48:09.65	–29:12:14.1	8.30	–3.34	16.88	0.008		
OW J080731.83–274915.1	08:07:31.83	–27:49:15.1	8.34	–3.29	17.08	0.004	0.82	0.60
OW J082109.09–292742.9	08:21:09.09	–29:27:42.9	8.69	–2.90	20.35	0.172		
OW J073951.17–270456.9	07:39:51.17	–27:04:56.9	8.82	–3.38	19.43	0.087	1.24	1.01
OW J081647.13–290504.8	08:16:47.13	–29:05:04.8	8.96	–2.92	18.11	0.012		
OW J080439.77–274347.1	08:04:39.77	–27:43:47.1	9.02	–3.04	18.09	0.008	0.84	0.64
OW J080907.97–295959.2	08:09:07.97	–29:59:59.2	10.11	–2.97	20.55	0.120	1.03	1.15
OW J073718.48–290854.8	07:37:18.48	–29:08:54.8	10.29	–2.83	17.08	0.004	1.01	0.60
OW J073910.05–294526.0	07:39:10.05	–29:45:26.0	10.55	–2.86	18.84	0.027	0.88	0.72
OW J081400.87–292214.0	08:14:00.87	–29:22:14.0	10.95	–2.72	21.18	0.326		
OW J081559.65–300415.7	08:15:59.65	–30:04:15.7	11.11	–2.74	20.22	0.075		
OW J074457.96–295837.1	07:44:57.96	–29:58:37.1	11.14	–3.61	20.98	0.288	1.71	
OW J080842.84–294515.4	08:08:42.84	–29:45:15.4	11.59	–2.89	19.53	0.034	1.04	0.59
OW J080609.07–293232.3	08:06:09.07	–29:32:32.3	12.07	–2.97	19.42	0.029	0.96	0.72
OW J081813.75–295236.3	08:18:13.75	–29:52:36.3	12.48	–2.79	20.12	0.073		
OW J080923.18–291234.3	08:09:23.18	–29:12:34.3	12.68	–2.81	17.57	0.006		
OW J075017.91–295749.0	07:50:17.91	–29:57:49.0	13.03	–2.85	19.79	0.033		
OW J075441.81–270712.3	07:54:41.81	–27:07:12.3	14.28	–2.93	21.00	0.178	1.82	
OW J075407.81–280408.4	07:54:07.81	–28:04:08.4	15.52	–2.75	18.96	0.027	0.93	0.78
OW J081332.46–294021.3	08:13:32.46	–29:40:21.3	16.43	–3.11	18.85	0.015		
OW J073919.72–300922.7	07:39:19.72	–30:09:22.7	17.38	–2.83	16.26	0.002	0.39	0.64
OW J074742.91–291239.3	07:47:42.91	–29:12:39.3	18.37	–2.57	19.99	0.046		
OW J074625.05–292609.9	07:46:25.05	–29:26:09.9	18.54	–2.62	21.37	0.202		
OW J075414.12–263626.2	07:54:14.12	–26:36:26.2	19.75	–2.85	17.01	0.004	0.86	0.50
OW J080638.35–300847.9	08:06:38.35	–30:08:47.9	19.82	–2.73	19.02	0.020	0.90	0.51
OW J074533.96–290100.0	07:45:33.96	–29:01:00.0	20.01	–2.55	21.05	0.193		
OW J075532.58–280854.3	07:55:32.58	–28:08:54.3	21.57	–4.17	16.70	0.008	0.49	0.68
OW J074106.07–294811.0	07:41:06.07	–29:48:11.0	22.56	–3.87	20.02	0.106	0.02	–1.0
OW J073941.78–291231.6	07:39:41.78	–29:12:31.6	23.01	–3.88	20.21	0.137	1.23	
OW J075823.42–292846.0	07:58:23.42	–29:28:46.0	23.30	–3.31	16.47	0.005		
OW J074320.76–294537.7	07:43:20.76	–29:45:37.7	23.32	–2.87	18.26	0.010	0.86	0.61
OW J081230.51–300025.3	08:12:30.51	–30:00:25.3	23.41	–2.76	21.16	0.308		
OW J074221.56–290844.2	07:42:21.56	–29:08:44.2	23.45	–4.08	16.42	0.005	0.37	0.64
OW J075516.35–270921.5	07:55:16.35	–27:09:21.5	23.64	–4.66	17.21	0.012	0.51	0.65
OW J080717.38–273614.2	08:07:17.38	–27:36:14.2	25.46	–3.03	19.84	0.055	1.05	1.04
OW J081803.46–300347.6	08:18:03.46	–30:03:47.6	26.18	–3.32	19.07	0.050		
OW J075359.78–275732.6	07:53:59.78	–27:57:32.6	26.19	–5.28	13.98	0.008	0.31	0.53
OW J081012.82–291529.2	08:10:12.82	–29:15:29.2	26.70	–3.14	16.64	0.007		
OW J082242.54–291609.1	08:22:42.54	–29:16:09.1	27.78	–2.97	18.52	0.061		
OW J074445.25–293137.0	07:44:45.25	–29:31:37.0	27.86	–3.56	20.74	0.147		
OW J080811.06–293708.8	08:08:11.06	–29:37:08.8	28.47	–2.69	16.14	0.011	0.59	0.67
OW J073703.84–261618.5	07:37:03.84	–26:16:18.5	29.09	–3.95	15.15	0.004		
OW J080114.78–300247.7	08:01:14.78	–30:02:47.7	29.33	–4.13	17.74	0.009		
OW J073739.20–291035.8	07:37:39.20	–29:10:35.8	29.34	–4.23	16.97	0.006	0.62	0.7
OW J080418.75–293740.2	08:04:18.75	–29:37:40.2	30.41	–3.37	14.17	0.002	0.25	0.45
OW J073841.20–265039.3	07:38:41.20	–26:50:39.3	30.50	–3.05	18.16	0.313	0.76	1.03
OW J074340.35–285833.6	07:43:40.35	–28:58:33.6	30.78	–2.52	16.87	0.071	0.95	0.69
OW J075710.04–264230.9	07:57:10.04	–26:42:30.9	30.90	–3.46	14.86	0.003		
OW J082113.71–291715.2	08:21:13.71	–29:17:15.2	31.00	–3.09	16.47	0.004		
OW J080916.72–292158.0	08:09:16.72	–29:21:58.0	31.14	–5.78	15.30	0.010	0.33	0.51
OW J073848.67–264628.0	07:38:48.67	–26:46:28.0	31.16	–3.11	17.95	0.166	1.18	1.42
OW J080611.57–300136.2	08:06:11.57	–30:01:36.2	31.96	–3.17	16.55	0.010	0.68	0.81

Table A2 – *continued* Parameters of the 613 variable candidates (selected using $n = 15$): star ID; RA and Dec; Lomb Scargle period (P_{LS}) and false alarm probability ($\log_{10}$(FAP)) of the highest peak in the periodogram, OW calibrated g-band magnitude, RMS of magnitude, VPHAS+ colour indices $g - r$ and $u - g$, and comments on variability type.

Star ID	RA (J2000) (hh:mm:ss)	DEC (J2000) (°:′:″)	P_{LS} (min)	$\log_{10}$(FAP)	OWg (mag)	RMS (mag)	$g - r$ (mag)	$u - g$ (mag)
OW J074908.65–275805.7	07:49:08.65	–27:58:05.7	32.18	–3.12	14.34	0.003	0.32	0.52
OW J080901.69–295231.7	08:09:01.69	–29:52:31.7	32.61	–4.08	14.59	0.005	0.26	0.52
OW J074233.32–261325.8	07:42:33.32	–26:13:25.8	33.87	–3.21	14.32	0.003	0.29	0.47
OW J080416.01–290712.7	08:04:16.01	–29:07:12.7	34.09	–3.02	16.54	0.006		
OW J074626.36–274840.5	07:46:26.36	–27:48:40.5	34.71	–3.02	16.50	0.005	1.51	1.65
OW J081106.60–273648.4	08:11:06.60	–27:36:48.4	35.48	–3.72	15.34	0.004		
OW J075846.54–280500.3	07:58:46.54	–28:05:00.3	35.87	–3.21	17.03	0.015	0.50	0.55
OW J073856.20–264626.4	07:38:56.20	–26:46:26.4	35.88	–4.75	18.85	0.304	1.08	0.63
OW J074315.36–264018.1	07:43:15.36	–26:40:18.1	35.90	–2.90	16.73	0.006	0.54	0.60
OW J075613.51–300614.0	07:56:13.51	–30:06:14.0	36.18	–3.46	15.52	0.003		
OW J074041.93–300645.3	07:40:41.93	–30:06:45.3	36.65	–3.23	19.73	0.101	0.94	0.60
OW J080152.94–271342.6	08:01:52.94	–27:13:42.6	36.69	–3.29	18.99	0.144		
OW J081545.99–292826.8	08:15:45.99	–29:28:26.8	36.94	–3.29	16.60	0.007		
OW J074411.20–294610.5	07:44:11.20	–29:46:10.5	37.22	–3.04	16.28	0.003	0.69	0.98
OW J073849.06–265135.9	07:38:49.06	–26:51:35.9	37.67	–3.52	17.04	0.065		
OW J075924.17–294252.6	07:59:24.17	–29:42:52.6	37.71	–3.81	17.49	0.015		
OW J075114.46–270311.2	07:51:14.46	–27:03:11.2	37.76	–3.72	15.69	0.004	0.65	0.51
OW J075952.17–292817.6	07:59:52.17	–29:28:17.6	38.18	–4.37	15.05	0.004		
OW J074513.22–261036.0	07:45:13.22	–26:10:36.0	38.19	–3.73	14.73	0.004	0.27	0.53
OW J080655.27–272608.0	08:06:55.27	–27:26:08.0	38.32	–3.02	15.02	0.004	0.41	0.38
OW J075640.83–291107.9	07:56:40.83	–29:11:07.9	38.71	–3.86	15.83	0.004		
OW J074106.40–293325.5	07:41:06.40	–29:33:25.5	38.81	–4.89	15.75	0.004	0.37	0.51
OW J074434.96–264808.9	07:44:34.96	–26:48:08.9	38.84	–3.90	16.12	0.008	0.43	0.59
OW J080824.49–271217.8	08:08:24.49	–27:12:17.8	38.86	–4.34	16.70	0.009	0.42	0.50
OW J075012.92–271148.0	07:50:12.92	–27:11:48.0	39.49	–3.22	14.54	0.004	0.44	0.60
OW J075748.59–294229.5	07:57:48.59	–29:42:29.5	39.63	–3.30	15.48	0.003		
OW J080605.59–292234.4	08:06:05.59	–29:22:34.4	39.68	–2.88	14.28	0.003	0.28	0.40
OW J080901.66–291652.2	08:09:01.66	–29:16:52.2	39.77	–3.62	16.24	0.007		
OW J074041.34–264257.1	07:40:41.34	–26:42:57.1	39.91	–3.88	14.82	0.003	0.47	0.55
OW J074436.59–300029.5	07:44:36.59	–30:00:29.5	40.16	–3.22	16.35	0.005	0.39	0.64
OW J074557.90–300516.7	07:45:57.90	–30:05:16.7	40.18	–2.95	15.37	0.009	0.40	0.61
OW J073856.23–264548.6	07:38:56.23	–26:45:48.6	40.19	–3.63	20.03	0.468	1.08	–0.1
OW J073939.81–265844.4	07:39:39.81	–26:58:44.4	40.34	–3.25	18.67	0.073	1.16	0.94
OW J075419.96–293704.3	07:54:19.96	–29:37:04.3	40.35	–3.53	15.82	0.004		
OW J074440.08–261253.7	07:44:40.08	–26:12:53.7	40.36	–3.30	15.98	0.007	0.53	0.56
OW J075121.36–270916.4	07:51:21.36	–27:09:16.4	40.37	–4.98	14.63	0.008	0.33	0.45
OW J073942.31–265713.7	07:39:42.31	–26:57:13.7	40.62	–3.15	20.22	0.448	1.64	
OW J073839.35–264802.4	07:38:39.35	–26:48:02.4	40.77	–3.74	15.92	0.016	1.06	1.28
OW J074124.13–292449.8	07:41:24.13	–29:24:49.8	40.94	–3.35	14.62	0.002	0.36	0.56
OW J074906.13–300320.4	07:49:06.13	–30:03:20.4	40.97	–3.12	17.31	0.008		
OW J074124.67–292654.7	07:41:24.67	–29:26:54.7	41.05	–4.48	15.29	0.003	0.42	0.56
OW J075133.98–271522.2	07:51:33.98	–27:15:22.2	41.52	–4.09	15.44	0.006	0.57	0.67
OW J074418.03–270139.9	07:44:18.03	–27:01:39.9	41.54	–4.08	14.42	0.005	0.36	0.42
OW J080711.45–291233.9	08:07:11.45	–29:12:33.9	41.83	–2.84	15.47	0.007		
OW J074152.52–300333.3	07:41:52.52	–30:03:33.3	41.87	–5.13	14.25	0.004	0.44	0.52
OW J073759.32–264105.9	07:37:59.32	–26:41:05.9	41.97	–3.85	14.00	0.003	0.34	0.32
OW J080035.88–273058.1	08:00:35.88	–27:30:58.1	42.01	–4.45	15.44	0.005	0.46	0.49
OW J075833.04–265711.9	07:58:33.04	–26:57:11.9	42.02	–3.50	15.74	0.005	0.53	0.72
OW J081148.15–300215.1	08:11:48.15	–30:02:15.1	42.06	–3.28	14.15	0.004		
OW J074234.58–261756.7	07:42:34.58	–26:17:56.7	42.31	–2.91	19.30	0.107	1.04	0.86
OW J074712.02–273212.3	07:47:12.02	–27:32:12.3	42.48	–3.91	14.91	0.004	0.47	0.73
OW J074515.87–295334.4	07:45:15.87	–29:53:34.4	42.72	–2.96	20.16	0.213	1.26	
OW J081609.09–285513.5	08:16:09.09	–28:55:13.5	42.79	–3.40	18.45	0.026		
OW J081154.63–273242.1	08:11:54.63	–27:32:42.1	42.80	–3.65	16.62	0.008		
OW J080954.62–271434.9	08:09:54.62	–27:14:34.9	42.80	–3.00	14.66	0.004	0.33	0.44
OW J074132.38–294608.7	07:41:32.38	–29:46:08.7	42.84	–3.28	17.54	0.009	0.41	0.62

Table A2 – *continued* Parameters of the 613 variable candidates (selected using $n = 15$): star ID; RA and Dec; Lomb Scargle period (P_{LS}) and false alarm probability ($\log_{10}$(FAP)) of the highest peak in the periodogram, OW calibrated g-band magnitude, RMS of magnitude, VPHAS+ colour indices $g - r$ and $u - g$, and comments on variability type.

Star ID	RA (J2000) (hh:mm:ss)	DEC (J2000) (°:′:″)	P_{LS} (min)	$\log_{10}$(FAP)	OWg (mag)	RMS (mag)	$g - r$ (mag)	$u - g$ (mag)
OW J073725.87–263356.4	07:37:25.87	–26:33:56.4	42.92	–3.59	15.16	0.004	0.50	0.57
OW J075313.21–273742.4	07:53:13.21	–27:37:42.4	42.99	–2.73	14.41	0.003	0.47	0.44
OW J080304.91–273919.9	08:03:04.91	–27:39:19.9	43.13	–4.31	17.61	0.012	0.44	0.58
OW J075804.98–293133.2	07:58:04.98	–29:31:33.2	43.15	–3.49	14.12	0.002		
OW J074637.60–274453.0	07:46:37.60	–27:44:53.0	43.23	–2.59	17.16	0.011	0.71	0.79
OW J074537.63–263020.0	07:45:37.63	–26:30:20.0	43.28	–2.85	15.96	0.007	0.48	0.61
OW J074539.69–295332.8	07:45:39.69	–29:53:32.8	43.35	–4.38	15.69	0.005	0.66	0.80
OW J073841.29–264929.0	07:38:41.29	–26:49:29.0	43.75	–3.49	18.56	0.462		
OW J082215.84–291633.1	08:22:15.84	–29:16:33.1	44.07	–3.52	14.36	0.006		
OW J074259.45–261534.3	07:42:59.45	–26:15:34.3	44.11	–4.43	14.64	0.004	0.28	0.59
OW J080516.63–294246.8	08:05:16.63	–29:42:46.8	44.12	–3.23	16.24	0.010	0.62	0.65
OW J074113.56–294236.4	07:41:13.56	–29:42:36.4	44.39	–3.86	14.88	0.003	0.42	0.45
OW J073857.26–264706.2	07:38:57.26	–26:47:06.2	44.78	–4.82	18.13	0.292	0.67	0.56
OW J073939.92–300506.7	07:39:39.92	–30:05:06.7	44.92	–3.56	14.22	0.003	0.43	0.53
OW J081409.59–285250.8	08:14:09.59	–28:52:50.8	45.08	–4.68	15.70	0.020		
OW J080036.71–300741.3	08:00:36.71	–30:07:41.3	45.31	–3.88	14.25	0.004		
OW J075509.29–261332.7	07:55:09.29	–26:13:32.7	45.32	–3.57	15.97	0.003		
OW J075319.28–292130.6	07:53:19.28	–29:21:30.6	45.67	–4.55	15.13	0.005		
OW J074343.56–295221.0	07:43:43.56	–29:52:21.0	46.06	–3.47	15.15	0.005	0.64	0.72
OW J074903.22–272649.3	07:49:03.22	–27:26:49.3	46.24	–3.34	15.46	0.005	0.62	0.74
OW J075112.07–291603.3	07:51:12.07	–29:16:03.3	46.32	–2.97	14.77	0.005		
OW J073857.23–265029.0	07:38:57.23	–26:50:29.0	46.37	–3.22	20.49	0.903	1.11	
OW J080417.88–271648.9	08:04:17.88	–27:16:48.9	46.60	–3.54	16.63	0.009		
OW J075633.52–300428.7	07:56:33.52	–30:04:28.7	46.60	–4.52	15.43	0.005	1.07	0.98
OW J080114.34–291022.6	08:01:14.34	–29:10:22.6	46.96	–4.08	19.51	0.217		
OW J080511.97–271648.6	08:05:11.97	–27:16:48.6	47.00	–2.93	16.76	0.013	0.46	0.51
OW J073848.26–264708.0	07:38:48.26	–26:47:08.0	47.20	–3.27	16.08	0.020	2.20	
OW J074236.74–261743.3	07:42:36.74	–26:17:43.3	47.23	–2.61	18.69	0.056	0.93	0.65
OW J073844.32–264957.6	07:38:44.32	–26:49:57.6	47.40	–3.73	20.18	0.370		
OW J075347.02–272159.5	07:53:47.02	–27:21:59.5	47.92	–3.16	16.40	0.004	0.55	0.62
OW J080527.94–275144.8	08:05:27.94	–27:51:44.8	48.03	–4.64	15.52	0.004	0.45	0.41
OW J073837.82–264813.3	07:38:37.82	–26:48:13.3	48.40	–3.56	15.99	0.016	0.77	0.53
OW J073835.96–264914.4	07:38:35.96	–26:49:14.4	48.61	–3.49	18.52	0.127	1.30	1.42
OW J073910.21–264538.4	07:39:10.21	–26:45:38.4	48.61	–3.52	16.79	0.010	0.84	0.81
OW J081014.26–300740.5	08:10:14.26	–30:07:40.5	48.69	–3.89	15.53	0.006	0.55	0.63
OW J073924.34–291540.8	07:39:24.34	–29:15:40.8	48.99	–5.02	15.23	0.004	0.63	0.67
OW J073852.94–264633.9	07:38:52.94	–26:46:33.9	49.03	–3.23	19.87	0.297	1.18	
OW J074047.63–294123.8	07:40:47.63	–29:41:23.8	49.15	–4.13	15.57	0.006	0.55	0.58
OW J074407.08–270310.4	07:44:07.08	–27:03:10.4	49.48	–4.25	14.67	0.005	0.43	0.47
OW J082209.22–294337.4	08:22:09.22	–29:43:37.4	49.65	–3.42	14.17	0.002		
OW J080034.92–280218.1	08:00:34.92	–28:02:18.1	49.78	–3.44	13.78	0.027	0.74	0.51
OW J080857.12–293427.1	08:08:57.12	–29:34:27.1	49.82	–3.98	15.61	0.005	0.40	0.62
OW J074644.24–291703.1	07:46:44.24	–29:17:03.1	49.87	–3.28	17.08	0.008		
OW J073838.23–264905.8	07:38:38.23	–26:49:05.8	49.89	–4.91	18.85	0.386	1.11	0.87
OW J074316.36–293438.2	07:43:16.36	–29:34:38.2	50.13	–4.44	15.40	0.018	0.59	0.71
OW J081112.36–270905.1	08:11:12.36	–27:09:05.1	50.45	–5.42	17.73	0.021		
OW J074549.33–291055.2	07:45:49.33	–29:10:55.2	50.47	–3.91	16.75	0.008		
OW J073836.43–264918.6	07:38:36.43	–26:49:18.6	50.55	–4.44	17.97	0.102	0.97	0.96
OW J075157.29–271344.5	07:51:57.29	–27:13:44.5	50.57	–4.20	17.90	0.022	0.74	0.93
OW J080347.30–295511.3	08:03:47.30	–29:55:11.3	50.63	–3.69	15.14	0.005	0.39	0.48
OW J073839.82–265007.5	07:38:39.82	–26:50:07.5	51.01	–5.26	17.81	0.110	0.80	0.81
OW J074158.69–264424.8	07:41:58.69	–26:44:24.8	51.04	–3.77	16.50	0.010	0.70	0.66
OW J080603.68–273807.6	08:06:03.68	–27:38:07.6	51.16	–4.18	15.50	0.011	0.45	0.47
OW J080522.72–272112.4	08:05:22.72	–27:21:12.4	51.16	–4.20	15.73	0.008	0.48	0.38
OW J074832.78–271804.4	07:48:32.78	–27:18:04.4	51.45	–3.57	15.30	0.003		
OW J074007.59–270017.6	07:40:07.59	–27:00:17.6	51.47	–3.81	16.60	0.009	0.66	0.80

Table A2 – *continued* Parameters of the 613 variable candidates (selected using $n = 15$): star ID; RA and Dec; Lomb Scargle period (P_{LS}) and false alarm probability ($\log_{10}$(FAP)) of the highest peak in the periodogram, OW calibrated g-band magnitude, RMS of magnitude, VPHAS+ colour indices $g - r$ and $u - g$, and comments on variability type.

Star ID	RA (J2000) (hh:mm:ss)	DEC (J2000) (°:′:″)	P_{LS} (min)	$\log_{10}$(FAP)	OWg (mag)	RMS (mag)	$g - r$ (mag)	$u - g$ (mag)
OW J073842.50–264752.1	07:38:42.50	–26:47:52.1	51.47	–3.98	16.01	0.018	0.62	0.75
OW J074017.09–294217.3	07:40:17.09	–29:42:17.3	51.49	–3.52	19.90	0.067	1.18	1.36
OW J074343.36–295605.4	07:43:43.36	–29:56:05.4	51.53	–4.74	15.79	0.007	0.64	0.80
OW J074209.66–294726.9	07:42:09.66	–29:47:26.9	51.53	–3.68	16.19	0.004	0.59	0.65
OW J074316.36–293113.8	07:43:16.36	–29:31:13.8	51.71	–3.58	18.67	0.031	0.95	0.74
OW J080550.52–275257.5	08:05:50.52	–27:52:57.5	51.88	–3.10	17.14	0.008	0.62	0.59
OW J074451.56–293454.2	07:44:51.56	–29:34:54.2	51.89	–3.64	14.88	0.004	0.58	0.66
OW J074304.26–261301.6	07:43:04.26	–26:13:01.6	51.97	–3.80	13.86	0.003	0.35	0.51
OW J075841.13–273338.9	07:58:41.13	–27:33:38.9	52.08	–3.12	18.17	0.022	1.49	1.71
OW J075828.38–272520.8	07:58:28.38	–27:25:20.8	52.32	–3.06	14.04	0.023		
OW J073752.46–294141.9	07:37:52.46	–29:41:41.9	52.56	–4.11	19.61	0.102	1.09	0.89
OW J081018.30–273749.1	08:10:18.30	–27:37:49.1	52.63	–4.94	15.49	0.014	0.41	0.44
OW J075639.02–271703.9	07:56:39.02	–27:17:03.9	52.81	–2.80	13.95	0.026	0.61	0.36
OW J073830.12–293053.3	07:38:30.12	–29:30:53.3	52.93	–6.10	17.47	0.012	0.76	0.89
OW J080406.85–291059.2	08:04:06.85	–29:10:59.2	52.93	–4.69	17.96	0.067		
OW J081947.35–294936.8	08:19:47.35	–29:49:36.8	53.01	–4.53	15.68	0.007		
OW J075850.74–272649.9	07:58:50.74	–27:26:49.9	53.05	–3.08	14.06	0.028		
OW J075633.35–292756.6	07:56:33.35	–29:27:56.6	53.20	–4.58	13.86	0.003		
OW J081744.68–293258.4	08:17:44.68	–29:32:58.4	53.25	–3.99	15.93	0.007		
OW J075637.82–271624.3	07:56:37.82	–27:16:24.3	53.30	–2.96	13.84	0.032	0.62	0.43
OW J080440.12–272645.5	08:04:40.12	–27:26:45.5	53.39	–2.87	16.42	0.005		
OW J081047.03–272143.5	08:10:47.03	–27:21:43.5	53.65	–3.91	20.13	0.087	0.64	0.42
OW J080247.11–290527.4	08:02:47.11	–29:05:27.4	54.23	–3.13	14.34	0.004		
OW J073851.40–265038.1	07:38:51.40	–26:50:38.1	54.69	–3.31	18.30	0.245	1.05	0.83
OW J075821.70–290813.5	07:58:21.70	–29:08:13.5	54.70	–4.23	19.03	0.049		
OW J074355.31–285728.4	07:43:55.31	–28:57:28.4	54.76	–3.05	17.46	0.147		
OW J075223.68–271639.2	07:52:23.68	–27:16:39.2	55.15	–2.82	16.14	0.015	0.60	0.50
OW J073701.39–291943.1	07:37:01.39	–29:19:43.1	55.25	–4.73	14.02	0.007	0.41	0.61
OW J081025.13–293541.9	08:10:25.13	–29:35:41.9	55.25	–3.57	15.27	0.007	0.36	0.37
OW J073955.32–265229.3	07:39:55.32	–26:52:29.3	55.76	–4.60	16.63	0.013		
OW J074932.47–274925.1	07:49:32.47	–27:49:25.1	55.98	–2.92	19.36	0.114	1.17	1.67
OW J073841.17–264825.8	07:38:41.17	–26:48:25.8	56.03	–4.16	19.18	0.563	1.02	0.58
OW J081015.61–280338.9	08:10:15.61	–28:03:38.9	56.12	–4.62	17.62	0.021	0.55	0.55
OW J081258.61–272021.7	08:12:58.61	–27:20:21.7	56.12	–3.79	17.42	0.009		
OW J075629.98–294045.3	07:56:29.98	–29:40:45.3	56.29	–3.94	13.89	0.004		
OW J074314.31–264949.6	07:43:14.31	–26:49:49.6	56.34	–3.48	14.44	0.004	0.30	0.30
OW J080918.09–274757.1	08:09:18.09	–27:47:57.1	56.41	–3.77	16.47	0.008	0.53	0.54
OW J075427.21–273230.1	07:54:27.21	–27:32:30.1	56.43	–4.77	16.34	0.008	0.63	0.61
OW J081024.53–294638.8	08:10:24.53	–29:46:38.8	56.49	–3.22	15.11	0.004	0.42	0.58
OW J081007.87–292101.7	08:10:07.87	–29:21:01.7	56.49	–3.45	16.92	0.010	0.53	0.48
OW J073932.84–265631.1	07:39:32.84	–26:56:31.1	56.59	–3.89	19.03	0.141	1.57	1.69
OW J073845.66–265204.5	07:38:45.66	–26:52:04.5	56.59	–4.56	16.33	0.012	0.67	0.72
OW J073852.17–265057.6	07:38:52.17	–26:50:57.6	56.59	–3.96	16.89	0.030	0.70	0.46
OW J074552.16–300109.5	07:45:52.16	–30:01:09.5	56.68	–5.69	14.86	0.015	0.44	0.79
OW J074432.46–292035.3	07:44:32.46	–29:20:35.3	56.90	–5.44	15.55	0.005		
OW J075638.90–294502.5	07:56:38.90	–29:45:02.5	57.11	–3.55	14.21	0.003		
OW J080116.39–290855.3	08:01:16.39	–29:08:55.3	57.33	–2.57	17.77	0.018		
OW J074246.21–265445.4	07:42:46.21	–26:54:45.4	57.48	–3.29	14.76	0.004	1.24	1.26
OW J080646.87–273439.6	08:06:46.87	–27:34:39.6	57.89	–3.46	14.79	0.006	0.47	0.42
OW J080303.10–293040.7	08:03:03.10	–29:30:40.7	57.94	–3.77	17.73	0.013	0.77	0.84
OW J075137.19–273052.0	07:51:37.19	–27:30:52.0	58.00	–3.40	17.35	0.011	0.71	0.65
OW J074500.26–262056.5	07:45:00.26	–26:20:56.5	58.37	–3.67	15.72	0.004	0.61	0.43
OW J074902.90–275010.5	07:49:02.90	–27:50:10.5	58.68	–3.17	16.52	0.009	0.96	1.12
OW J075620.67–291605.4	07:56:20.67	–29:16:05.4	58.84	–4.31	16.95	0.016		
OW J074434.05–264907.6	07:44:34.05	–26:49:07.6	58.97	–3.53	16.50	0.008	0.57	0.65
OW J074108.72–291003.0	07:41:08.72	–29:10:03.0	59.13	–5.78	16.41	0.012	0.39	0.80

Table A2 – *continued* Parameters of the 613 variable candidates (selected using $n = 15$): star ID; RA and Dec; Lomb Scargle period (P_{LS}) and false alarm probability ($\log_{10}$(FAP)) of the highest peak in the periodogram, OW calibrated g-band magnitude, RMS of magnitude, VPHAS+ colour indices $g - r$ and $u - g$, and comments on variability type.

Star ID	RA (J2000) (hh:mm:ss)	DEC (J2000) (°:′:″)	P_{LS} (min)	$\log_{10}$(FAP)	OWg (mag)	RMS (mag)	$g - r$ (mag)	$u - g$ (mag)
OW J075009.03–292023.1	07:50:09.03	–29:20:23.1	59.21	–3.14	17.39	0.009		
OW J074924.79–280357.8	07:49:24.79	–28:03:57.8	59.40	–2.98	17.01	0.009	0.87	0.96
OW J080008.72–293132.7	08:00:08.72	–29:31:32.7	59.72	–4.36	19.19	0.087		
OW J074029.02–300434.9	07:40:29.02	–30:04:34.9	60.07	–3.96	19.48	0.381		0.68
OW J080310.43–290316.8	08:03:10.43	–29:03:16.8	60.08	–3.43	13.76	0.011		
OW J081102.39–291220.8	08:11:02.39	–29:12:20.8	60.15	–4.18	16.60	0.012		
OW J073651.88–264330.0	07:36:51.88	–26:43:30.0	60.18	–3.45	14.10	0.003	0.31	0.35
OW J073843.16–264931.1	07:38:43.16	–26:49:31.1	60.18	–3.85	18.56	0.226	1.35	1.12
OW J073748.28–262741.6	07:37:48.28	–26:27:41.6	60.18	–2.97	14.15	0.005		
OW J081627.93–293642.7	08:16:27.93	–29:36:42.7	60.28	–4.34	15.71	0.006		
OW J073956.88–295532.6	07:39:56.88	–29:55:32.6	60.31	–3.44	15.67	0.004	0.63	0.70
OW J074050.39–293721.1	07:40:50.39	–29:37:21.1	60.31	–3.70	14.39	0.004	0.49	0.58
OW J080523.11–283933.7	08:05:23.11	–28:39:33.7	60.38	–3.07	17.41	0.014		
OW J073925.95–265513.4	07:39:25.95	–26:55:13.4	60.50	–3.65	18.35	0.051	1.01	0.65
OW J074150.69–293936.9	07:41:50.69	–29:39:36.9	60.65	–3.75	18.15	0.011	0.60	0.62
OW J080456.78–285031.1	08:04:56.78	–28:50:31.1	60.74	–2.94	16.84	0.010		
OW J075749.04–270714.3	07:57:49.04	–27:07:14.3	60.82	–3.76	16.66	0.006	0.73	0.76
OW J080714.84–293311.9	08:07:14.84	–29:33:11.9	60.95	–4.87	14.05	0.004	0.36	0.47
OW J074211.98–292453.2	07:42:11.98	–29:24:53.2	61.15	–3.07	14.57	0.004	0.17	–0.0
OW J073939.52–265750.8	07:39:39.52	–26:57:50.8	61.16	–3.14	19.57	0.155	0.96	1.08
OW J074016.01–294201.6	07:40:16.01	–29:42:01.6	61.29	–3.75	17.67	0.013	0.92	0.77
OW J074310.62–300811.3	07:43:10.62	–30:08:11.3	61.41	–4.79	17.14	0.009	0.62	0.59
OW J081016.66–294119.8	08:10:16.66	–29:41:19.8	61.41	–3.44	15.77	0.005	0.59	0.65
OW J080627.53–275142.9	08:06:27.53	–27:51:42.9	61.44	–3.55	18.17	0.020	0.59	0.70
OW J075806.20–264333.3	07:58:06.20	–26:43:33.3	61.47	–4.91	17.66	0.017	0.70	0.86
OW J074638.44–293249.8	07:46:38.44	–29:32:49.8	61.61	–3.29	18.45	0.018	0.99	0.85
OW J074320.83–292132.2	07:43:20.83	–29:21:32.2	61.92	–3.18	20.43	0.144	0.85	0.59
OW J073828.32–300407.7	07:38:28.32	–30:04:07.7	62.04	–4.09	20.22	0.339	1.28	
OW J075710.05–263815.3	07:57:10.05	–26:38:15.3	62.13	–4.11	18.29	0.022		
OW J074759.81–273307.3	07:47:59.81	–27:33:07.3	62.18	–3.09	17.57	0.011	0.87	0.93
OW J074329.11–270001.3	07:43:29.11	–27:00:01.3	62.19	–3.56	15.15	0.004	0.53	0.51
OW J080646.48–294233.7	08:06:46.48	–29:42:33.7	62.24	–3.51	15.98	0.005	0.52	0.55
OW J074152.26–300558.6	07:41:52.26	–30:05:58.6	62.45	–4.48	20.03	0.284	1.12	
OW J075303.88–274734.8	07:53:03.88	–27:47:34.8	62.46	–2.86	16.52	0.006	0.67	0.73
OW J080416.29–280611.7	08:04:16.29	–28:06:11.7	62.49	–3.92	15.97	0.005	0.50	0.53
OW J080458.07–274612.6	08:04:58.07	–27:46:12.6	62.49	–3.29	16.27	0.010	0.47	0.52
OW J080955.62–292436.8	08:09:55.62	–29:24:36.8	62.50	–4.14	14.24	0.006	0.40	0.45
OW J080729.17–293417.1	08:07:29.17	–29:34:17.1	62.68	–5.19	17.00	0.012	0.52	0.52
OW J081144.93–291023.0	08:11:44.93	–29:10:23.0	63.17	–4.10	20.07	0.088		
OW J080606.67–273737.2	08:06:06.67	–27:37:37.2	63.21	–3.09	15.44	0.006		
OW J075404.32–272228.6	07:54:04.32	–27:22:28.6	63.27	–4.09	16.45	0.007	0.60	0.58
OW J073954.47–294857.4	07:39:54.47	–29:48:57.4	63.34	–3.94	20.52	0.261	0.91	0.43
OW J081011.14–295552.1	08:10:11.14	–29:55:52.1	63.40	–3.80	16.18	0.007	0.62	0.82
OW J080733.15–294044.8	08:07:33.15	–29:40:44.8	63.57	–5.44	16.71	0.009	0.58	0.65
OW J080643.56–271048.7	08:06:43.56	–27:10:48.7	63.58	–3.55	17.32	0.017	0.63	0.65
OW J081102.18–271045.4	08:11:02.18	–27:10:45.4	63.58	–3.69	17.21	0.009		
OW J080919.75–292036.7	08:09:19.75	–29:20:36.7	63.63	–3.21	15.83	0.005		
OW J081431.99–293015.1	08:14:31.99	–29:30:15.1	63.78	–4.77	14.76	0.008		
OW J080817.42–274834.9	08:08:17.42	–27:48:34.9	64.32	–4.30	16.23	0.010	0.47	0.48
OW J081547.93–290929.0	08:15:47.93	–29:09:29.0	64.53	–3.59	14.99	0.006		
OW J075507.97–270738.1	07:55:07.97	–27:07:38.1	64.56	–5.52	17.05	0.015	0.65	0.52
OW J080435.95–275150.7	08:04:35.95	–27:51:50.7	64.70	–3.25	14.37	0.008	0.43	0.41
OW J074618.64–294846.7	07:46:18.64	–29:48:46.7	64.95	–3.03	19.90	0.076	0.77	0.68
OW J080711.60–294222.9	08:07:11.60	–29:42:22.9	64.97	–3.54	19.25	0.342	0.88	0.91
OW J081147.86–293130.3	08:11:47.86	–29:31:30.3	65.04	–4.05	16.62	0.006		
OW J075317.49–275043.7	07:53:17.49	–27:50:43.7	65.25	–4.61	17.00	0.012	0.63	0.69

Table A2 – *continued* Parameters of the 613 variable candidates (selected using $n = 15$): star ID; RA and Dec; Lomb Scargle period (P_{LS}) and false alarm probability ($\log_{10}$(FAP)) of the highest peak in the periodogram, OW calibrated g-band magnitude, RMS of magnitude, VPHAS+ colour indices $g - r$ and $u - g$, and comments on variability type.

Star ID	RA (J2000) (hh:mm:ss)	DEC (J2000) (°:′:″)	P_{LS} (min)	$\log_{10}$(FAP)	OWg (mag)	RMS (mag)	$g - r$ (mag)	$u - g$ (mag)
OW J075026.49–273513.6	07:50:26.49	–27:35:13.6	65.54	–4.43	15.20	0.004	0.50	0.52
OW J080625.13–293011.0	08:06:25.13	–29:30:11.0	65.69	–4.71	15.90	0.008	0.53	0.45
OW J074033.58–263001.7	07:40:33.58	–26:30:01.7	65.75	–3.93	14.67	0.009		
OW J074517.66–264834.6	07:45:17.66	–26:48:34.6	65.79	–3.07	15.91	0.005	0.56	0.48
OW J074352.62–300512.2	07:43:52.62	–30:05:12.2	65.79	–4.46	15.70	0.005	0.61	0.66
OW J073843.80–293811.7	07:38:43.80	–29:38:11.7	65.82	–4.57	16.24	0.004	0.80	0.77
OW J081354.15–284643.9	08:13:54.15	–28:46:43.9	66.00	–3.86	15.68	0.010		
OW J081754.77–283831.0	08:17:54.77	–28:38:31.0	66.00	–3.59	20.11	0.287		
OW J081024.73–292038.4	08:10:24.73	–29:20:38.4	66.01	–4.77	15.04	0.009	0.41	0.48
OW J074514.02–261929.5	07:45:14.02	–26:19:29.5	66.17	–4.08	14.27	0.004	0.32	0.44
OW J080433.65–294123.0	08:04:33.65	–29:41:23.0	66.18	–4.31	14.33	0.005	0.37	0.56
OW J080620.15–280339.7	08:06:20.15	–28:03:39.7	66.26	–3.53	17.30	0.008	0.54	0.67
OW J074253.18–291419.0	07:42:53.18	–29:14:19.0	66.39	–5.29	18.43	0.027	0.76	0.73
OW J074354.26–270716.7	07:43:54.26	–27:07:16.7	66.56	–3.13	16.70	0.008	0.73	0.73
OW J074523.26–261716.4	07:45:23.26	–26:17:16.4	66.56	–4.28	15.50	0.006	0.46	0.56
OW J075928.98–290837.4	07:59:28.98	–29:08:37.4	66.58	–4.77	16.22	0.008		
OW J074242.65–295053.8	07:42:42.65	–29:50:53.8	66.69	–5.22	20.10	0.093	0.77	0.90
OW J074240.27–294136.6	07:42:40.27	–29:41:36.6	66.69	–4.19	16.10	0.004	0.53	0.62
OW J080836.38–284322.1	08:08:36.38	–28:43:22.1	66.82	–3.22	16.21	0.019		
OW J074455.63–261640.2	07:44:55.63	–26:16:40.2	66.95	–3.60	15.15	0.005	0.60	0.65
OW J074100.72–293854.9	07:41:00.72	–29:38:54.9	67.28	–4.27	16.77	0.007	0.48	0.51
OW J074119.49–270558.7	07:41:19.49	–27:05:58.7	67.35	–3.92	14.71	0.003	0.50	0.57
OW J074202.43–295134.1	07:42:02.43	–29:51:34.1	67.61	–5.13	14.13	0.002	0.34	0.37
OW J074129.37–291152.8	07:41:29.37	–29:11:52.8	67.61	–4.06	16.30	0.006	0.57	0.66
OW J075144.20–294920.4	07:51:44.20	–29:49:20.4	67.75	–4.34	18.54	0.022		
OW J074406.83–295723.2	07:44:06.83	–29:57:23.2	67.92	–3.56	20.61	0.442	1.24	
OW J073845.42–264919.6	07:38:45.42	–26:49:19.6	68.11	–4.35	18.82	0.585	1.16	
OW J073726.08–291709.5	07:37:26.08	–29:17:09.5	68.19	–3.73	17.57	0.008	0.92	1.01
OW J073843.63–265053.8	07:38:43.63	–26:50:53.8	68.52	–5.28	18.53	0.215	1.14	1.37
OW J075845.70–291247.9	07:58:45.70	–29:12:47.9	68.54	–5.08	16.97	0.012		
OW J080842.12–285633.7	08:08:42.12	–28:56:33.7	68.65	–2.63	16.23	0.008		
OW J074628.87–294103.4	07:46:28.87	–29:41:03.4	68.68	–4.05	16.07	0.008	0.74	0.89
OW J080850.48–272110.3	08:08:50.48	–27:21:10.3	68.74	–3.62	16.14	0.009	0.60	0.51
OW J073938.57–265457.8	07:39:38.57	–26:54:57.8	68.94	–3.18	19.97	0.319	1.02	0.81
OW J080510.58–273100.8	08:05:10.58	–27:31:00.8	69.17	–3.44	15.80	0.006	0.40	0.42
OW J073842.90–264902.5	07:38:42.90	–26:49:02.5	69.36	–3.28	17.68	0.191		0.84
OW J073849.04–264710.8	07:38:49.04	–26:47:10.8	69.36	–3.25	17.38	0.159	1.67	
OW J081116.89–293257.3	08:11:16.89	–29:32:57.3	69.39	–4.35	16.76	0.007		
OW J080636.44–271646.1	08:06:36.44	–27:16:46.1	69.61	–4.12	17.51	0.011	0.62	0.56
OW J081035.55–280225.8	08:10:35.55	–28:02:25.8	69.61	–3.27	20.04	0.091	0.69	0.59
OW J073654.65–262659.8	07:36:54.65	–26:26:59.8	69.78	–3.12	15.76	0.006		
OW J081249.26–292054.4	08:12:49.26	–29:20:54.4	69.94	–4.92	18.54	0.043		
OW J075320.94–264238.5	07:53:20.94	–26:42:38.5	70.03	–4.74	18.59	0.101	1.05	0.56
OW J073656.97–291333.2	07:36:56.97	–29:13:33.2	70.08	–3.60	16.35	0.005	0.62	0.68
OW J073910.45–263917.7	07:39:10.45	–26:39:17.7	70.22	–3.42	15.25	0.006	0.62	0.62
OW J081020.64–291017.6	08:10:20.64	–29:10:17.6	70.22	–3.87	17.12	0.021		
OW J073906.66–291117.4	07:39:06.66	–29:11:17.4	70.41	–3.91	19.49	0.063	1.42	1.03
OW J081034.02–271621.4	08:10:34.02	–27:16:21.4	70.51	–3.78	17.74	0.020	0.60	0.56
OW J080754.01–292702.8	08:07:54.01	–29:27:02.8	70.67	–4.61	14.92	0.007	0.45	0.65
OW J073940.84–300725.4	07:39:40.84	–30:07:25.4	70.74	–4.40	16.00	0.007	0.66	0.79
OW J074053.11–300111.6	07:40:53.11	–30:01:11.6	70.74	–3.15	18.64	0.080	0.92	0.71
OW J082009.02–291839.3	08:20:09.02	–29:18:39.3	70.79	–5.56	15.86	0.013		
OW J074314.35–284824.1	07:43:14.35	–28:48:24.1	70.81	–3.32	14.33	0.008	0.48	0.60
OW J073912.51–295906.4	07:39:12.51	–29:59:06.4	71.07	–3.27	18.59	0.017	0.68	0.90
OW J080818.31–290051.5	08:08:18.31	–29:00:51.5	71.08	–3.79	17.54	0.019		
OW J074403.79–292106.2	07:44:03.79	–29:21:06.2	71.20	–5.06	16.06	0.007		

Table A2 – *continued* Parameters of the 613 variable candidates (selected using $n = 15$): star ID; RA and Dec; Lomb Scargle period (P_{LS}) and false alarm probability ($\log_{10}$(FAP)) of the highest peak in the periodogram, OW calibrated g-band magnitude, RMS of magnitude, VPHAS+ colour indices $g - r$ and $u - g$, and comments on variability type.

Star ID	RA (J2000) (hh:mm:ss)	DEC (J2000) (°:′:″)	P_{LS} (min)	$\log_{10}$(FAP)	OWg (mag)	RMS (mag)	$g - r$ (mag)	$u - g$ (mag)
OW J073929.00–295950.4	07:39:29.00	–29:59:50.4	71.40	–3.63	16.32	0.008	0.70	0.74
OW J081119.48–280105.0	08:11:19.48	–28:01:05.0	71.42	–4.54	17.36	0.019		
OW J080835.00–272656.8	08:08:35.00	–27:26:56.8	71.89	–3.81	16.23	0.020	0.49	0.63
OW J075907.07–263950.5	07:59:07.07	–26:39:50.5	72.23	–3.96	18.83	0.053	0.85	0.48
OW J075449.09–261721.2	07:54:49.09	–26:17:21.2	72.23	–3.65	17.42	0.010		
OW J080836.11–290207.3	08:08:36.11	–29:02:07.3	72.63	–3.02	16.47	0.006		
OW J074105.58–292956.1	07:41:05.58	–29:29:56.1	72.78	–4.57	16.10	0.006	0.54	0.53
OW J081138.83–280551.3	08:11:38.83	–28:05:51.3	72.84	–4.40	16.73	0.011		
OW J074402.56–285912.3	07:44:02.56	–28:59:12.3	73.06	–2.54	19.10	0.399		
OW J082239.39–300331.5	08:22:39.39	–30:03:31.5	73.15	–4.45	15.78	0.006		
OW J075957.78–292648.7	07:59:57.78	–29:26:48.7	73.24	–5.36	15.96	0.007		
OW J075218.07–271623.0	07:52:18.07	–27:16:23.0	73.44	–4.53	19.33	0.071	0.83	0.59
OW J075131.72–261359.9	07:51:31.72	–26:13:59.9	73.59	–6.02	14.89	0.027	0.37	0.56
OW J082105.69–294403.6	08:21:05.69	–29:44:03.6	73.64	–3.87	14.89	0.006		
OW J074453.47–292845.0	07:44:53.47	–29:28:45.0	73.69	–4.22	19.05	0.041		
OW J080501.05–281430.7	08:05:01.05	–28:14:30.7	73.69	–3.29	17.10	0.017	0.62	0.72
OW J080531.16–274221.5	08:05:31.16	–27:42:21.5	73.82	–4.93	17.59	0.020	0.55	0.60
OW J074533.75–263212.5	07:45:33.75	–26:32:12.5	73.91	–5.11	15.16	0.011	0.38	0.55
OW J074431.34–300030.2	07:44:31.34	–30:00:30.2	74.06	–5.97	14.54	0.003	0.46	0.58
OW J081957.09–292114.8	08:19:57.09	–29:21:14.8	74.14	–3.69	17.68	0.050		
OW J074235.05–261903.5	07:42:35.05	–26:19:03.5	74.39	–3.47	19.57	0.180	1.10	0.82
OW J074515.73–260841.7	07:45:15.73	–26:08:41.7	74.39	–5.35	15.11	0.009	0.49	0.56
OW J081733.99–283403.3	08:17:33.99	–28:34:03.3	74.53	–3.94	14.89	0.014		
OW J075709.77–261332.2	07:57:09.77	–26:13:32.2	74.56	–4.37	17.55	0.021		
OW J074028.01–294119.6	07:40:28.01	–29:41:19.6	74.57	–4.76	15.47	0.004	0.54	0.58
OW J081237.22–270929.9	08:12:37.22	–27:09:29.9	74.82	–5.06	17.75	0.083		
OW J074258.64–290554.4	07:42:58.64	–29:05:54.4	75.05	–2.62	15.60	0.014	0.69	
OW J073653.05–295851.6	07:36:53.05	–29:58:51.6	75.31	–5.42	18.13	0.016	0.76	0.69
OW J073937.05–295321.8	07:39:37.05	–29:53:21.8	75.69	–6.01	17.94	0.028	0.72	0.67
OW J080404.48–293424.3	08:04:04.48	–29:34:24.3	76.12	–4.65	15.09	0.005	0.51	0.67
OW J080907.24–291028.5	08:09:07.24	–29:10:28.5	76.13	–4.88	15.10	0.009		
OW J074808.04–293926.1	07:48:08.04	–29:39:26.1	76.17	–3.29	19.16	0.081		
OW J075646.36–274944.6	07:56:46.36	–27:49:44.6	76.35	–3.81	17.67	0.021	0.83	0.97
OW J081258.89–274655.4	08:12:58.89	–27:46:55.4	76.38	–4.16	16.37	0.010		
OW J073929.62–292153.2	07:39:29.62	–29:21:53.2	76.84	–4.49	16.62	0.006	0.58	0.52
OW J073759.97–261354.0	07:37:59.97	–26:13:54.0	76.86	–5.46	14.99	0.005		
OW J080750.27–274227.1	08:07:50.27	–27:42:27.1	76.91	–4.56	14.43	0.005	0.43	0.51
OW J075855.97–275525.2	07:58:55.97	–27:55:25.2	77.40	–4.08	19.30	0.065	1.11	0.84
OW J074437.39–270007.5	07:44:37.39	–27:00:07.5	77.42	–4.61	15.01	0.008	0.59	0.54
OW J075500.07–295913.3	07:55:00.07	–29:59:13.3	77.43	–3.72	16.72	0.008		
OW J074333.27–282219.7	07:43:33.27	–28:22:19.7	78.23	–3.19	20.02	0.188	0.95	1.51
OW J081519.24–292715.8	08:15:19.24	–29:27:15.8	78.36	–4.69	17.94	0.130		
OW J082056.71–293522.0	08:20:56.71	–29:35:22.0	78.37	–4.73	16.06	0.022		
OW J074458.44–261812.6	07:44:58.44	–26:18:12.6	78.49	–5.51	14.46	0.010	0.49	0.60
OW J080952.02–280623.1	08:09:52.02	–28:06:23.1	78.56	–3.85	16.40	0.007	0.55	0.60
OW J081053.86–272043.1	08:10:53.86	–27:20:43.1	78.56	–4.68	16.81	0.015		
OW J074611.10–300043.3	07:46:11.10	–30:00:43.3	78.67	–4.50	15.01	0.012	0.58	0.64
OW J073640.48–262430.0	07:36:40.48	–26:24:30.0	78.99	–4.66	15.08	0.006		
OW J080409.11–280057.5	08:04:09.11	–28:00:57.5	79.13	–4.45	15.65	0.006	0.37	0.54
OW J081057.63–271515.5	08:10:57.63	–27:15:15.5	79.13	–3.58	17.08	0.010		
OW J080720.01–292200.1	08:07:20.01	–29:22:00.1	79.18	–4.39	15.45	0.006	0.59	0.74
OW J082126.94–292700.7	08:21:26.94	–29:27:00.7	79.51	–4.14	14.75	0.006		
OW J073852.60–264930.4	07:38:52.60	–26:49:30.4	79.54	–5.06	14.98	0.013		
OW J073940.51–293944.7	07:39:40.51	–29:39:44.7	79.67	–6.57	13.65	0.009	0.49	0.57
OW J081145.14–275748.0	08:11:45.14	–27:57:48.0	79.70	–3.91	14.42	0.006		
OW J080959.20–271730.1	08:09:59.20	–27:17:30.1	79.70	–3.68	15.95	0.006	0.46	0.59

Table A2 – *continued* Parameters of the 613 variable candidates (selected using $n = 15$): star ID; RA and Dec; Lomb Scargle period (P_{LS}) and false alarm probability ($\log_{10}$(FAP)) of the highest peak in the periodogram, OW calibrated g-band magnitude, RMS of magnitude, VPHAS+ colour indices $g - r$ and $u - g$, and comments on variability type.

Star ID	RA (J2000) (hh:mm:ss)	DEC (J2000) (°:′:″)	P_{LS} (min)	$\log_{10}$(FAP)	OWg (mag)	RMS (mag)	$g - r$ (mag)	$u - g$ (mag)
OW J081258.21–300829.3	08:12:58.21	–30:08:29.3	79.75	–4.66	15.68	0.020		
OW J081243.44–274754.9	08:12:43.44	–27:47:54.9	80.28	–4.33	17.10	0.009		
OW J080909.14–273354.5	08:09:09.14	–27:33:54.5	80.28	–3.68	17.05	0.010	0.60	0.58
OW J081334.04–300054.5	08:13:34.04	–30:00:54.5	80.48	–4.36	19.67	0.160		
OW J074317.66–300712.2	07:43:17.66	–30:07:12.2	80.53	–6.60	15.03	0.006	0.54	0.85
OW J081557.95–293824.6	08:15:57.95	–29:38:24.6	80.66	–5.27	15.04	0.007		
OW J082209.66–292850.6	08:22:09.66	–29:28:50.6	80.68	–4.22	18.35	0.045		
OW J080042.43–274410.3	08:00:42.43	–27:44:10.3	80.72	–4.80	15.38	0.019	0.53	0.54
OW J075734.23–265848.5	07:57:34.23	–26:58:48.5	80.81	–4.12	18.75	0.046	1.01	1.17
OW J081540.61–293543.2	08:15:40.61	–29:35:43.2	81.26	–5.14	15.02	0.008		
OW J081501.94–291831.1	08:15:01.94	–29:18:31.1	81.87	–5.17	16.62	0.013		
OW J080648.77–271819.5	08:06:48.77	–27:18:19.5	82.08	–4.93	17.36	0.020	0.66	0.62
OW J074403.53–285823.3	07:44:03.53	–28:58:23.3	82.19	–2.71	19.32	0.283		
OW J082002.87–292450.7	08:20:02.87	–29:24:50.7	82.50	–4.28	16.50	0.009		
OW J080821.26–293035.7	08:08:21.26	–29:30:35.7	82.50	–4.82	15.53	0.009	0.66	0.64
OW J075737.46–261142.1	07:57:37.46	–26:11:42.1	82.54	–3.94	20.53	0.319		
OW J074420.77–284406.2	07:44:20.77	–28:44:06.2	82.69	–2.92	15.49	0.013		
OW J080431.42–274151.2	08:04:31.42	–27:41:51.2	82.70	–4.84	16.81	0.027	0.57	0.65
OW J081106.84–272728.2	08:11:06.84	–27:27:28.2	82.70	–4.12	16.89	0.010		
OW J075811.50–275935.6	07:58:11.50	–27:59:35.6	83.09	–4.46	14.98	0.011	0.63	0.67
OW J075836.16–270954.2	07:58:36.16	–27:09:54.2	83.09	–3.83	16.12	0.010	0.63	0.59
OW J081840.30–293641.5	08:18:40.30	–29:36:41.5	83.76	–5.24	16.24	0.013		
OW J081950.24–293431.5	08:19:50.24	–29:34:31.5	83.76	–4.67	14.19	0.007		
OW J081130.03–280217.9	08:11:30.03	–28:02:17.9	83.96	–3.30	19.90	0.421		
OW J080749.50–300727.5	08:07:49.50	–30:07:27.5	84.06	–4.21	16.01	0.008	0.56	0.65
OW J074125.63–291144.2	07:41:25.63	–29:11:44.2	84.22	–6.09	16.37	0.008	0.54	0.67
OW J073953.24–261017.6	07:39:53.24	–26:10:17.6	84.26	–5.83	13.69	0.006	0.43	0.48
OW J074219.36–270614.5	07:42:19.36	–27:06:14.5	84.31	–4.65	15.64	0.008	0.95	–0.0
OW J075815.66–274811.8	07:58:15.66	–27:48:11.8	84.33	–4.32	15.33	0.011	0.46	0.38
OW J082225.32–300216.9	08:22:25.32	–30:02:16.9	84.40	–4.97	15.70	0.014		
OW J082040.56–292638.2	08:20:40.56	–29:26:38.2	84.40	–5.40	16.42	0.016		
OW J074238.25–270008.2	07:42:38.25	–27:00:08.2	84.94	–4.16	15.06	0.004	0.69	0.73
OW J074829.63–292935.9	07:48:29.63	–29:29:35.9	85.06	–3.09	15.82	0.008		
OW J074935.56–281952.1	07:49:35.56	–28:19:52.1	85.14	–2.96	17.83	0.030	1.06	1.16
OW J074126.58–282452.9	07:41:26.58	–28:24:52.9	85.25	–4.16	17.18	0.027	0.86	1.01
OW J074521.56–265501.4	07:45:21.56	–26:55:01.4	85.57	–4.96	16.99	0.018	0.68	0.72
OW J082206.07–300833.7	08:22:06.07	–30:08:33.7	85.72	–5.22	16.67	0.014		
OW J080112.55–290907.4	08:01:12.55	–29:09:07.4	85.75	–2.98	19.64	0.804		
OW J074657.64–270910.3	07:46:57.64	–27:09:10.3	85.95	–4.98	16.50	0.012	0.60	0.57
OW J080711.98–294621.7	08:07:11.98	–29:46:21.7	86.10	–4.67	17.54	0.023	0.67	0.78
OW J075841.75–265118.4	07:58:41.75	–26:51:18.4	86.24	–4.01	14.64	0.007	0.49	0.68
OW J080337.48–274426.6	08:03:37.48	–27:44:26.6	86.93	–5.26	14.37	0.020	0.37	0.53
OW J081700.03–294221.9	08:17:00.03	–29:42:21.9	87.07	–5.22	15.91	0.015		
OW J074114.01–285030.6	07:41:14.01	–28:50:30.6	87.47	–2.68	21.13	0.965	1.14	
OW J074211.66–270025.6	07:42:11.66	–27:00:25.6	87.55	–4.57	14.91	0.008	0.53	0.51
OW J075554.58–280000.6	07:55:54.58	–28:00:00.6	87.60	–5.33	14.88	0.009	0.54	0.61
OW J074216.26–290655.6	07:42:16.26	–29:06:55.6	87.95	–2.81	20.47	0.586	1.44	
OW J073924.57–265051.9	07:39:24.57	–26:50:51.9	88.18	–4.37	18.27	0.189		
OW J073936.73–262212.5	07:39:36.73	–26:22:12.5	88.18	–3.93	16.66	0.011		
OW J074140.92–300040.8	07:41:40.92	–30:00:40.8	88.25	–6.27	15.14	0.013	0.58	0.61
OW J075458.98–271708.9	07:54:58.98	–27:17:08.9	88.29	–3.66	19.40	0.083	1.46	1.25
OW J075610.47–272149.5	07:56:10.47	–27:21:49.5	88.29	–3.65	20.93	0.923	1.23	
OW J075629.30–273027.0	07:56:29.30	–27:30:27.0	88.98	–4.75	18.10	0.022	0.94	0.92
OW J075501.55–271519.2	07:55:01.55	–27:15:19.2	88.98	–4.53	16.52	0.013	0.88	0.84
OW J081336.63–292728.7	08:13:36.63	–29:27:28.7	89.01	–4.14	17.66	0.017		
OW J080733.14–275849.0	08:07:33.14	–27:58:49.0	89.42	–4.20	16.66	0.013	0.53	0.54

Table A2 – *continued* Parameters of the 613 variable candidates (selected using $n = 15$): star ID; RA and Dec; Lomb Scargle period (P_{LS}) and false alarm probability ($\log_{10}$(FAP)) of the highest peak in the periodogram, OW calibrated g-band magnitude, RMS of magnitude, VPHAS+ colour indices $g - r$ and $u - g$, and comments on variability type.

Star ID	RA (J2000) (hh:mm:ss)	DEC (J2000) (°:′:″)	P_{LS} (min)	$\log_{10}$(FAP)	OWg (mag)	RMS (mag)	$g - r$ (mag)	$u - g$ (mag)
OW J073909.96–300620.0	07:39:09.96	–30:06:20.0	89.57	–5.92	13.64	0.004	0.48	0.55
OW J075007.25–290929.5	07:50:07.25	–29:09:29.5	89.61	–4.09	18.30	0.028		
OW J074438.06–293024.4	07:44:38.06	–29:30:24.4	89.87	–5.37	16.23	0.015		
OW J080951.45–280013.6	08:09:51.45	–28:00:13.6	90.16	–3.36	17.08	0.013	0.67	0.66
OW J081234.75–280445.8	08:12:34.75	–28:04:45.8	90.16	–3.88	20.61	0.190		
OW J075142.86–274827.4	07:51:42.86	–27:48:27.4	90.22	–3.71	14.79	0.003		
OW J075530.25–262524.6	07:55:30.25	–26:25:24.6	90.28	–3.73	15.09	0.005		
OW J074403.60–265046.4	07:44:03.60	–26:50:46.4	90.33	–4.62	16.38	0.011		
OW J081656.53–290708.7	08:16:56.53	–29:07:08.7	90.54	–2.73	20.40	0.364		
OW J081445.93–283722.8	08:14:45.93	–28:37:22.8	90.54	–3.23	19.61	0.071		
OW J081659.84–281421.7	08:16:59.84	–28:14:21.7	90.54	–3.36	16.86	0.012		
OW J074855.83–284153.6	07:48:55.83	–28:41:53.6	90.74	–3.24	15.41	0.016	1.03	0.66
OW J074645.93–280508.3	07:46:45.93	–28:05:08.3	91.32	–4.49	18.83	0.058	0.91	0.80
OW J080110.68–272425.5	08:01:10.68	–27:24:25.5	91.88	–4.88	18.21	0.028		
OW J074342.43–282124.2	07:43:42.43	–28:21:24.2	91.90	–3.56	16.65	0.018	1.01	0.86
OW J075356.45–280521.1	07:53:56.45	–28:05:21.1	91.92	–4.17	16.50	0.008	0.44	0.72
OW J074501.15–264111.4	07:45:01.15	–26:41:11.4	92.53	–3.17	19.18	0.131	0.97	0.84
OW J074855.79–284154.8	07:48:55.79	–28:41:54.8	93.19	–3.46	16.34	0.042		
OW J080522.52–274530.1	08:05:22.52	–27:45:30.1	93.21	–4.27	16.04	0.007	0.45	0.45
OW J073845.45–265022.1	07:38:45.45	–26:50:22.1	93.24	–5.56	17.93	0.195	1.01	0.90
OW J074347.36–284456.4	07:43:47.36	–28:44:56.4	93.30	–2.51	19.33	0.102		
OW J074618.67–295901.9	07:46:18.67	–29:59:01.9	93.61	–3.72	17.44	0.014	0.62	0.61
OW J080710.90–280427.0	08:07:10.90	–28:04:27.0	94.00	–4.25	18.24	0.034	0.69	0.75
OW J081020.02–295947.6	08:10:20.02	–29:59:47.6	94.25	–3.76	16.89	0.013	0.77	0.86
OW J075940.00–283413.4	07:59:40.00	–28:34:13.4	94.65	–2.89	15.75	0.021	0.69	0.55
OW J074558.70–293954.0	07:45:58.70	–29:39:54.0	94.67	–3.48	18.45	0.025	0.86	0.74
OW J073836.30–261928.9	07:38:36.30	–26:19:28.9	94.79	–4.99	16.54	0.028		
OW J080811.07–271919.5	08:08:11.07	–27:19:19.5	94.81	–4.06	17.05	0.017	0.62	0.63
OW J074510.96–292255.4	07:45:10.96	–29:22:55.4	95.08	–5.15	15.80	0.006		
OW J075008.60–291735.3	07:50:08.60	–29:17:35.3	95.21	–3.61	19.92	0.381		
OW J081107.77–290909.1	08:11:07.77	–29:09:09.1	95.27	–3.44	18.46	0.026		
OW J073851.43–264900.0	07:38:51.43	–26:49:00.0	95.44	–4.14	19.75	0.753		
OW J080403.70–280617.5	08:04:03.70	–28:06:17.5	95.64	–3.62	20.82	0.330	1.25	
OW J075304.79–295329.8	07:53:04.79	–29:53:29.8	95.64	–3.59	15.82	0.006		
OW J074401.15–294309.1	07:44:01.15	–29:43:09.1	95.70	–6.94	13.53	0.008	0.51	0.70
OW J074654.84–292037.1	07:46:54.84	–29:20:37.1	95.75	–5.07	17.37	0.036		
OW J074734.94–281423.1	07:47:34.94	–28:14:23.1	96.10	–3.48	19.72	0.152	1.35	
OW J075323.63–274252.9	07:53:23.63	–27:42:52.9	96.15	–3.40	15.15	0.015	0.63	0.75
OW J074813.44–281912.8	07:48:13.44	–28:19:12.8	96.45	–3.83	18.42	0.225	0.83	0.83
OW J080721.49–272516.5	08:07:21.49	–27:25:16.5	96.48	–2.78	17.84	0.013	0.78	0.71
OW J080933.49–272637.3	08:09:33.49	–27:26:37.3	96.48	–3.79	19.85	0.120		
OW J074732.66–291828.0	07:47:32.66	–29:18:28.0	96.86	–4.37	16.53	0.012		
OW J080529.37–280242.6	08:05:29.37	–28:02:42.6	97.33	–3.36	20.13	0.190	0.91	0.47
OW J075814.67–271045.6	07:58:14.67	–27:10:45.6	97.42	–5.42	19.05	0.093	0.90	0.78
OW J075332.00–280522.5	07:53:32.00	–28:05:22.5	97.44	–3.58	16.63	0.009	0.71	0.67
OW J075006.96–274227.7	07:50:06.96	–27:42:27.7	98.06	–3.96	17.21	0.011	0.93	1.05
OW J075120.91–273835.1	07:51:20.91	–27:38:35.1	98.09	–2.64	16.57	0.009	0.84	0.92
OW J074127.83–263628.9	07:41:27.83	–26:36:28.9	98.12	–5.28	14.20	0.005	0.60	0.65
OW J080418.12–280750.5	08:04:18.12	–28:07:50.5	98.20	–4.20	17.98	0.022	0.74	0.75
OW J080525.22–280229.5	08:05:25.22	–28:02:29.5	98.20	–3.44	20.96	1.010	1.35	
OW J080529.63–280241.0	08:05:29.63	–28:02:41.0	98.20	–4.12	20.77	0.391	1.26	
OW J081126.75–280146.6	08:11:26.75	–28:01:46.6	98.21	–3.60	14.97	0.008		
OW J074848.35–284053.0	07:48:48.35	–28:40:53.0	98.52	–2.64	19.35	0.076	1.66	1.54
OW J075328.54–293642.6	07:53:28.54	–29:36:42.6	98.52	–3.31	15.11	0.019		
OW J081355.65–283955.9	08:13:55.65	–28:39:55.9	98.70	–3.78	16.68	0.022		
OW J074412.75–263541.8	07:44:12.75	–26:35:41.8	98.97	–3.69	17.78	0.030	0.86	0.83

Table A2 – *continued* Parameters of the 613 variable candidates (selected using $n = 15$): star ID; RA and Dec; Lomb Scargle period (P_{LS}) and false alarm probability ($\log_{10}$(FAP)) of the highest peak in the periodogram, OW calibrated g-band magnitude, RMS of magnitude, VPHAS+ colour indices $g - r$ and $u - g$, and comments on variability type.

Star ID	RA (J2000) (hh:mm:ss)	DEC (J2000) (°:′:″)	P_{LS} (min)	$\log_{10}$(FAP)	OWg (mag)	RMS (mag)	$g - r$ (mag)	$u - g$ (mag)
OW J075221.80–293027.7	07:52:21.80	–29:30:27.7	99.14	–3.41	15.65	0.005		
OW J075031.81–294516.7	07:50:31.81	–29:45:16.7	99.15	–3.53	14.84	0.006		
OW J074606.57–295609.2	07:46:06.57	–29:56:09.2	99.74	–3.50	15.71	0.003	0.49	0.65
OW J075011.62–291209.3	07:50:11.62	–29:12:09.3	99.74	–4.44	17.04	0.017		
OW J075231.48–292530.5	07:52:31.48	–29:25:30.5	99.75	–3.54	17.67	0.015		
OW J080620.34–275230.0	08:06:20.34	–27:52:30.0	99.99	–4.01	17.32	0.008	0.63	0.55
OW J080607.93–271319.7	08:06:07.93	–27:13:19.7	99.99	–3.97	15.66	0.007	0.44	0.64
OW J080642.71–271247.3	08:06:42.71	–27:12:47.3	99.99	–4.48	16.47	0.008	0.61	0.57
OW J080706.37–272024.4	08:07:06.37	–27:20:24.4	99.99	–3.48	18.82	0.151	0.92	0.49
OW J075348.08–280827.6	07:53:48.08	–28:08:27.6	100.10	–3.51	18.21	0.034	0.91	0.93
OW J075340.11–290933.0	07:53:40.11	–29:09:33.0	100.37	–4.21	17.07	0.019		
OW J080914.88–274906.9	08:09:14.88	–27:49:06.9	100.91	–4.66	17.07	0.014	0.64	0.78
OW J073905.75–294551.6	07:39:05.75	–29:45:51.6	100.92	–6.80	17.61	0.023	0.60	0.68
OW J074737.62–295622.8	07:47:37.62	–29:56:22.8	100.94	–3.72	20.37	0.565	1.73	
OW J073847.16–264935.9	07:38:47.16	–26:49:35.9	101.56	–4.98	18.64	0.166	1.17	0.47
OW J080456.26–275806.2	08:04:56.26	–27:58:06.2	101.84	–4.75	19.07	0.066	0.79	0.71
OW J080643.67–280647.5	08:06:43.67	–28:06:47.5	101.84	–4.33	16.17	0.006	0.57	0.48
OW J081256.71–280357.0	08:12:56.71	–28:03:57.0	101.84	–4.11	18.18	0.093		
OW J075006.61–281205.3	07:50:06.61	–28:12:05.3	102.17	–2.64	16.22	0.014	1.10	1.20
OW J074015.37–264404.7	07:40:15.37	–26:44:04.7	102.48	–4.70	14.61	0.006	0.67	0.79
OW J080220.45–274922.8	08:02:20.45	–27:49:22.8	102.74	–4.91	19.24	0.126	1.25	1.28
OW J081726.64–300138.9	08:17:26.64	–30:01:38.9	104.48	–4.28	17.61	0.054		
OW J074459.45–270412.1	07:44:59.45	–27:04:12.1	105.38	–5.42	15.89	0.012	0.57	0.52
OW J081735.27–294550.1	08:17:35.27	–29:45:50.1	105.48	–4.72	16.10	0.008		
OW J081728.79–294209.5	08:17:28.79	–29:42:09.5	105.48	–4.09	17.07	0.013		
OW J081506.97–292241.2	08:15:06.97	–29:22:41.2	105.48	–4.07	16.57	0.006		
OW J080549.71–284654.8	08:05:49.71	–28:46:54.8	105.50	–3.41	19.23	0.096		
OW J080538.14–284903.1	08:05:38.14	–28:49:03.1	105.50	–3.42	15.17	0.003		
OW J080748.48–280047.6	08:07:48.48	–28:00:47.6	105.76	–3.82	16.67	0.009	0.55	0.56
OW J080406.38–274331.7	08:04:06.38	–27:43:31.7	105.76	–4.91	17.51	0.018	0.52	0.59
OW J075824.90–275732.9	07:58:24.90	–27:57:32.9	106.61	–4.98	20.28	0.160	1.46	
OW J075002.67–275032.7	07:50:02.67	–27:50:32.7	106.65	–3.25	19.61	0.174	1.10	0.74
OW J080734.86–280152.4	08:07:34.86	–28:01:52.4	106.78	–4.98	15.36	0.017	0.49	0.48
OW J081208.49–274839.5	08:12:08.49	–27:48:39.5	106.79	–4.98	16.15	0.018		
OW J081216.27–271426.2	08:12:16.27	–27:14:26.2	106.79	–4.79	16.01	0.015		
OW J074831.08–290747.1	07:48:31.08	–29:07:47.1	106.92	–3.56	15.80	0.013		
OW J074827.36–281423.1	07:48:27.36	–28:14:23.1	107.63	–2.89	16.53	0.262		
OW J074918.47–281842.2	07:49:18.47	–28:18:42.2	107.63	–2.68	20.77	0.400	1.27	
OW J074827.26–281423.4	07:48:27.26	–28:14:23.4	107.76	–2.99	14.41	0.026	0.57	0.61
OW J075856.86–265916.7	07:58:56.86	–26:59:16.7	108.00	–4.36	18.30	0.054	0.87	0.89
OW J075858.94–261738.5	07:58:58.94	–26:17:38.5	108.00	–4.87	20.22	0.447		
OW J073859.23–262534.3	07:38:59.23	–26:25:34.3	108.33	–5.37	17.60	0.033		
OW J074606.22–284722.2	07:46:06.22	–28:47:22.2	108.50	–3.24	19.83	0.141	1.33	1.10
OW J075022.51–290342.1	07:50:22.51	–29:03:42.1	108.60	–2.84	18.32	0.138		
OW J080518.42–275048.5	08:05:18.42	–27:50:48.5	108.90	–5.31	14.81	0.014	0.45	0.51
OW J075502.20–262857.9	07:55:02.20	–26:28:57.9	109.02	–5.43	19.60	0.075		
OW J073838.88–264952.6	07:38:38.88	–26:49:52.6	109.37	–4.38	17.33	0.078		
OW J074827.12–281425.6	07:48:27.12	–28:14:25.6	109.47	–2.90	17.28	0.053	0.80	0.55
OW J080649.58–275653.7	08:06:49.58	–27:56:53.7	109.99	–4.50	17.42	0.016	0.52	0.71
OW J080539.25–274733.1	08:05:39.25	–27:47:33.1	109.99	–5.07	19.13	0.084	1.02	1.09
OW J080552.84–271634.2	08:05:52.84	–27:16:34.2	109.99	–4.80	15.72	0.022	0.52	0.40
OW J074825.52–291702.1	07:48:25.52	–29:17:02.1	110.97	–5.11	17.42	0.031		
OW J075340.29–261239.9	07:53:40.29	–26:12:39.9	111.10	–5.46	20.63	0.380	1.12	
OW J073703.63–262839.2	07:37:03.63	–26:28:39.2	111.52	–4.40	14.36	0.013		
OW J074957.17–295204.4	07:49:57.17	–29:52:04.4	111.71	–4.23	19.67	0.054		
OW J075847.06–264043.8	07:58:47.06	–26:40:43.8	112.20	–4.77	18.55	0.153	0.68	0.55

Table A2 – *continued* Parameters of the 613 variable candidates (selected using $n = 15$): star ID; RA and Dec; Lomb Scargle period (P_{LS}) and false alarm probability ($\log_{10}$(FAP)) of the highest peak in the periodogram, OW calibrated g-band magnitude, RMS of magnitude, VPHAS+ colour indices $g - r$ and $u - g$, and comments on variability type.

Star ID	RA (J2000) (hh:mm:ss)	DEC (J2000) (°:′:″)	P_{LS} (min)	$\log_{10}$(FAP)	OWg (mag)	RMS (mag)	$g - r$ (mag)	$u - g$ (mag)
OW J075802.18–263737.7	07:58:02.18	–26:37:37.7	112.20	–5.49	17.73	0.107	0.79	0.70
OW J080951.01–275210.3	08:09:51.01	–27:52:10.3	112.24	–4.14	19.98	0.140	1.00	0.64
OW J074714.30–291929.2	07:47:14.30	–29:19:29.2	112.46	–4.65	17.29	0.013		
OW J074745.86–271601.8	07:47:45.86	–27:16:01.8	113.27	–5.38	17.77	0.053	1.06	1.06
OW J081143.07–275147.1	08:11:43.07	–27:51:47.1	113.39	–4.00	16.24	0.014		
OW J081247.13–272220.9	08:12:47.13	–27:22:20.9	113.39	–5.64	19.15	0.100		
OW J081226.83–291413.8	08:12:26.83	–29:14:13.8	113.71	–5.60	15.57	0.015		
OW J080524.72–280334.2	08:05:24.72	–28:03:34.2	114.57	–4.87	19.52	0.168	0.96	0.56
OW J074054.27–262208.1	07:40:54.27	–26:22:08.1	114.90	–4.74	19.09	0.145	0.99	0.11
OW J074924.43–282011.5	07:49:24.43	–28:20:11.5	114.94	–4.02	17.82	0.154	1.01	1.21
OW J074909.15–272115.1	07:49:09.15	–27:21:15.1	115.05	–3.95	16.06	0.007	0.87	0.87
OW J075044.33–273018.7	07:50:44.33	–27:30:18.7	115.08	–3.95	17.06	0.017	0.87	0.85
OW J080402.96–275245.2	08:04:02.96	–27:52:45.2	115.77	–5.37	14.89	0.011	0.57	0.54
OW J080626.93–271139.8	08:06:26.93	–27:11:39.8	115.77	–5.71	15.38	0.007	0.56	0.51
OW J080932.11–270917.3	08:09:32.11	–27:09:17.3	115.78	–3.04	16.27	0.013	0.59	0.62
OW J074701.90–275114.8	07:47:01.90	–27:51:14.8	115.96	–4.36	14.77	0.010	0.58	0.57
OW J075307.08–300158.0	07:53:07.08	–30:01:58.0	116.14	–4.87	15.49	0.011		
OW J073826.18–295336.3	07:38:26.18	–29:53:36.3	116.44	–6.09	16.70	0.007	0.75	0.86
OW J074558.82–271706.0	07:45:58.82	–27:17:06.0	116.89	–3.83	18.02	0.027	0.94	0.84
OW J081021.38–274501.3	08:10:21.38	–27:45:01.3	117.01	–5.36	14.81	0.012	0.53	0.58
OW J081152.99–273055.1	08:11:52.99	–27:30:55.1	117.01	–5.31	20.18	0.486		
OW J081022.77–271934.6	08:10:22.77	–27:19:34.6	117.01	–5.14	16.67	0.028		
OW J074756.52–294425.7	07:47:56.52	–29:44:25.7	117.18	–3.05	18.84	0.019	1.18	1.01
OW J075434.58–273327.0	07:54:34.58	–27:33:27.0	117.87	–4.05	14.97	0.005	0.50	0.70
OW J081042.17–272524.1	08:10:42.17	–27:25:24.1	118.27	–4.56	15.15	0.014	0.57	0.48
OW J080922.63–271132.2	08:09:22.63	–27:11:32.2	118.27	–4.18	17.71	0.076	0.93	0.56
OW J074135.50–263709.6	07:41:35.50	–26:37:09.6	118.56	–5.97	16.32	0.063	0.66	0.64
OW J081117.93–275217.2	08:11:17.93	–27:52:17.2	119.55	–5.47	16.15	0.025		
OW J081148.09–273114.6	08:11:48.09	–27:31:14.6	119.55	–5.05	17.30	0.027		
OW J081101.90–271820.6	08:11:01.90	–27:18:20.6	119.55	–4.11	15.18	0.030		
OW J073936.74–263915.8	07:39:36.74	–26:39:15.8	121.01	–5.92	15.60	0.015	0.73	0.80
OW J074922.65–272040.2	07:49:22.65	–27:20:40.2	121.76	–4.34	14.30	0.004	0.46	0.60
OW J080659.36–271325.7	08:06:59.36	–27:13:25.7	122.21	–4.53	17.13	0.015	0.96	0.86
OW J075420.79–292521.3	07:54:20.79	–29:25:21.3	122.25	–5.17	17.68	0.023		
OW J075217.31–273114.9	07:52:17.31	–27:31:14.9	122.82	–3.10	20.18	0.161	1.36	
OW J075402.13–272654.2	07:54:02.13	–27:26:54.2	122.82	–4.55	15.97	0.009	0.73	0.74
OW J073809.52–291603.9	07:38:09.52	–29:16:03.9	123.07	–6.95	15.43	0.019	0.75	0.73
OW J080743.56–275803.8	08:07:43.56	–27:58:03.8	124.98	–4.97	18.80	0.077	0.85	0.63
OW J080815.43–271824.8	08:08:15.43	–27:18:24.8	124.98	–4.56	17.77	0.044	0.97	0.64
OW J075136.90–294437.6	07:51:36.90	–29:44:37.6	125.07	–4.76	17.49	0.040		
OW J081828.59–293148.6	08:18:28.59	–29:31:48.6	126.12	–5.19	18.96	0.094		
OW J073731.43–262213.3	07:37:31.43	–26:22:13.3	126.39	–5.67	14.54	0.013		
OW J080817.17–293454.1	08:08:17.17	–29:34:54.1	127.61	–4.66	19.43	0.085	1.00	0.89
OW J074938.92–273704.3	07:49:38.92	–27:37:04.3	128.17	–5.57	15.15	0.013	0.84	0.97
OW J075920.14–280220.0	07:59:20.14	–28:02:20.0	128.41	–5.57	17.82	0.026	0.92	0.88
OW J074617.48–271936.2	07:46:17.48	–27:19:36.2	129.30	–5.08	18.03	0.062	0.79	0.80
OW J075044.98–274045.6	07:50:44.98	–27:40:45.6	129.34	–5.63	16.20	0.015	1.12	1.19
OW J080743.65–275805.4	08:07:43.65	–27:58:05.4	129.39	–4.34	19.82	0.152	0.92	
OW J075020.15–275754.2	07:50:20.15	–27:57:54.2	131.67	–4.37	20.05	0.242		
OW J075542.87–260949.6	07:55:42.87	–26:09:49.6	132.83	–5.89	15.05	0.060		
OW J074550.84–275823.7	07:45:50.84	–27:58:23.7	132.83	–3.19	16.19	0.005	0.74	0.46
OW J074813.07–271110.2	07:48:13.07	–27:11:10.2	132.83	–3.20	20.55	0.615	1.44	
OW J075023.21–275919.2	07:50:23.21	–27:59:19.2	132.87	–4.81	16.97	0.014	1.19	1.29